

Influence of lithology on hillslope morphology and response to tectonic forcing in the northern Sierra Nevada of California

Martin D. Hurst,^{1,2} Simon M. Mudd,^{1,3} Kyungsoo Yoo,⁴ Mikael Attal,¹ and Rachel Walcott^{1,5}

Received 6 February 2012; revised 13 February 2013; accepted 15 February 2013; published 24 May 2013.

[1] Many geomorphic studies assume that bedrock geology is not a first-order control on landscape form in order to isolate drivers of geomorphic change (e.g., climate or tectonics). Yet underlying geology may influence the efficacy of soil production and sediment transport on hillslopes. We performed quantitative analysis of LiDAR digital terrain models to examine the topographic form of hillslopes in two distinct lithologies in the Feather River catchment in northern California, a granodiorite pluton and metamorphosed volcanics. The two sites, separated by <2 km and spanning similar elevations, were assumed to have similar climatic histories and are experiencing a transience in landscape evolution characterized by a propagating incision wave in response to accelerated surface uplift c. 5 Ma. Responding to increased incision rates, hillslopes in granodiorite tend to have morphology similar to model predictions for steady state hillslopes, suggesting that they adjust rapidly to keep pace with the incision wave. By contrast, hillslopes in metavolcanics exhibit high gradients but lower hilltop curvature indicative of ongoing transient adjustment to incision. We used existing erosion rate data and the curvature of hilltops proximal to the main channels (where hillslopes have most likely adjusted to accelerated erosion rates) to demonstrate that the sediment transport coefficient is higher in granodiorite ($8.8 \text{ m}^2 \text{ ka}^{-1}$) than in metavolcanics ($4.8 \text{ m}^2 \text{ ka}^{-1}$). Hillslopes in both lithologies get shorter (i.e., drainage density increases) with increasing erosion rates.

Citation: Hurst, M. D., S. M. Mudd, K. Yoo, M. Attal, and R. Walcott (2013), Influence of lithology on hillslope morphology and response to tectonic forcing in the northern Sierra Nevada of California, *J. Geophys. Res. Earth Surf.*, 118, 832–851, doi:10.1002/jgrf.20049.

1. Introduction

[2] Climate and tectonics act in concert to control the morphology of the Earth's surface. The ability to quantify relationships between topography and climatic or tectonic driving processes is dependent on understanding how efficiently, and by which processes, sediment is generated and transported on hillslopes and in valleys [e.g., Ahnert, 1970; Dietrich *et al.*, 2003]. Such knowledge is vital for ongoing

modeling efforts which help link empirical observations to theoretical predictions [e.g., Tucker and Hancock, 2010]. Hillslope processes control the flux and caliber of sediment supplied to streams [e.g., Whittaker *et al.*, 2010], which subsequently influence fluvial incision rates [e.g., Sklar and Dietrich, 2004] and the rate at which sediment is delivered to basins [e.g., Duller *et al.*, 2010; Armitage *et al.*, 2011].

[3] Tectonic processes redistribute rock mass within the lithosphere and control the type and flux of rock material exhumed to the surface. This material may be weakened at depth via mechanical fracturing due to tectonic processes [e.g., Molnar *et al.*, 2007] and later disrupted at/near the surface by physical and chemical weathering processes (e.g., penetration and growth of tree roots [Roering *et al.*, 2010; Gabet and Mudd, 2010], frost wedging [e.g., Small *et al.*, 1999], and chemical alteration and weakening [e.g., Burke *et al.*, 2007; Dixon *et al.*, 2009]). These processes generate soil/regolith, here used synonymously and defined as material at or near the Earth's surface that is being physically disturbed (equivalent to the physically disturbed zone as defined by Yoo and Mudd [2008]) and which can be subsequently transported away. The type and physical properties (composition, rock mass strength, and degree of fracturing) of bedrock will influence the physical properties of the resulting soil (e.g., composition, grain size distribution,

¹School of Geosciences, University of Edinburgh, Edinburgh, UK.

²British Geological Survey, Nottingham, UK.

³Earth Research Institute, University of California, Santa Barbara, California, USA.

⁴Department of Soil, Water, and Climate, University of Minnesota, St. Paul, Minnesota, USA.

⁵Department of Natural Sciences, National Museums Scotland, Edinburgh, UK.

Corresponding author: M. D. Hurst, British Geological Survey, Nicker Hill, Keyworth, Nottingham NG12 5GG, UK. (mhurst@bgs.ac.uk)

©2013 The Authors. *Journal of Geophysical Research: Earth Surface* published by Wiley on behalf of the American Geophysical Union. This is an open access article under the terms of the Creative Commons Attribution License, which permits use, distribution and reproduction in any medium, provided the original work is properly cited. 2169-9003/13/10.1002/jgrf.20049

degree of weathering, porosity, and cohesion [Yoo *et al.*, 2005]). The physical characteristics of soil are in turn expected to influence the efficacy at which sediment transport occurs on hillslopes [Furbish *et al.*, 2009]. Thus, there is the potential for bedrock lithology to influence topography even in soil-mantled landscapes.

[4] Several studies have attempted to quantify relationships between rock strength and topography, or have considered the role that spatially variable rock type may have in controlling processes which generate and redistribute sediment at the Earth's surface. Schmidt and Montgomery [1995] demonstrated that hillslope relief is limited by the material strength of bedrock. Similarly, Burbank *et al.* [1996] suggested that hillslope gradients were limited at their internal friction angle, despite variation of over an order of magnitude in denudation rates in the northwest Himalayas ($1\text{--}12 \text{ mm a}^{-1}$). Hillslopes were thus interpreted to evolve in response to variable erosion rates by adjusting the frequency of landslides rather than by steepening. The distribution of slope angles may serve as a proxy for rock mass strength in landslide-dominated terrain as demonstrated by Korup [2008] and Korup and Schlunegger [2009]. Clarke and Burbank [2010] however were not able to distinguish rock mass strength from hillslope gradients in distinct lithologies in Southern New Zealand. They attributed the similarities between low-grade metamorphics of the Southern Alps and high-grade and igneous units of the Fiordland to the nature of bedrock fracturing. Both sites are susceptible to landsliding, but different styles of fracturing were interpreted to control the type of mass wasting process operating. In Fiordland, fracturing occurs primarily due to near surface processes and thus drives frequent shallow landslides, whereas pervasive tectonic fracturing in the Southern Alps facilitates larger, deeper landslides [Clarke and Burbank, 2010; 2011]. Although links between bedrock lithology and topography have been explored in bedrock landscapes, no studies have explored the role that lithology may play in controlling topography in soil-mantled landscapes.

[5] Lithology may play an important role in controlling the efficiency of sediment transport on hillslopes. McKean *et al.* [1993] showed that the sediment transport coefficient D , which relates hillslope gradient to sediment flux, is an order of magnitude larger in weak clay-rich soils than in strong, granular soils, presumably due to variation in the efficiency of shrink-swell cycles as a transport process. This is at least partially controlled by the parent lithology through the nature of jointing and susceptibility to weathering. Furbish *et al.* [2009] described the sediment transport coefficient D as a function of the material properties of soil including thickness, grain size distribution, and cohesion which may directly influence the efficiency of sediment transport. The presence of coarse material in the soil may result in a boulder lag which armours underlying soil from erosion [e.g., Granger *et al.*, 2001]. Owen *et al.*, 2010 demonstrated that hillslope erosion rates across a climate gradient in Chile were sensitive to precipitation, which influences transport processes, with more rapid erosion rate attributed to wetter climate and biologically driven sediment transport. To assess whether there is any existing evidence that D might be influenced by lithology, we compiled published values of D to search for global trends with lithology (Figure 1a and Table 1). Simplifying to cohesionless, clastic,

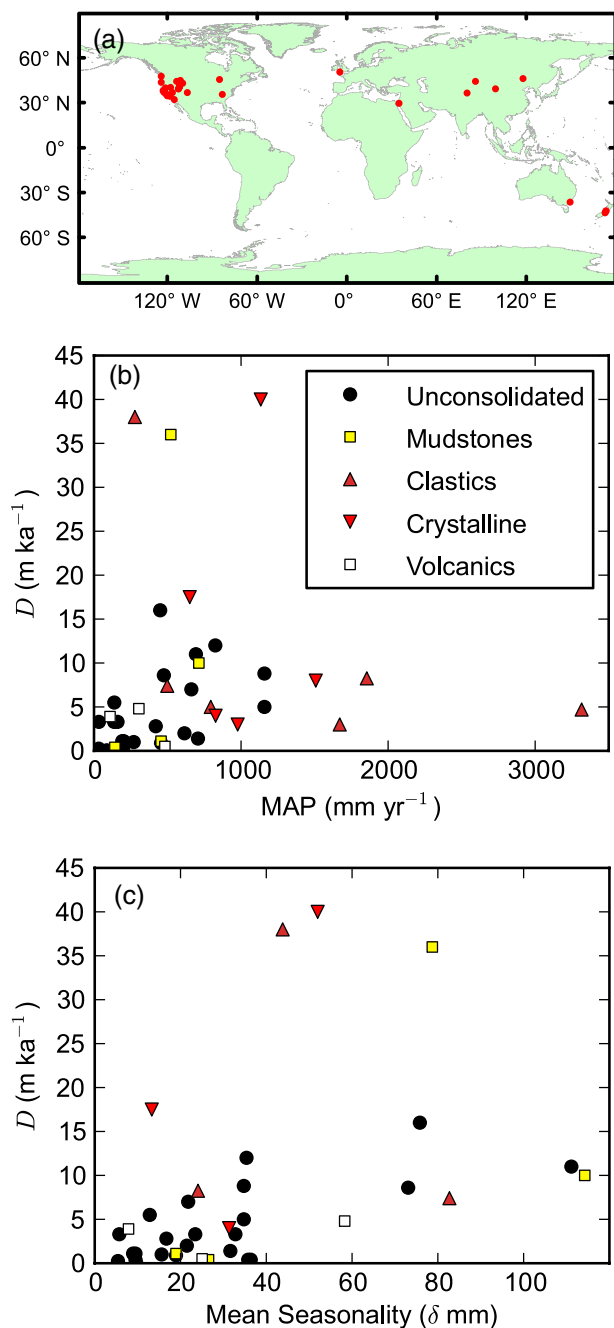


Figure 1. (a) Global distribution of calibrated sediment transport coefficients (red) (Table 1). (b) Mean annual precipitation plotted against calibrated sediment transport coefficients for lithologic groups. In unconsolidated substrate, there is a weak tendency for D to increase with wetter climate ($R^2=0.27$ for linear regression). (c) Sediment transport efficiency vs. annual variability of precipitation (2σ about mean monthly precipitation). D increases with more variable intra-annual precipitation ($R^2=0.51$ for linear regression). There were no trends observed when comparing D to mean annual temperature.

volcanic, and crystalline lithologic groups, we were not able to observe any trends between lithology and the sediment transport coefficient (Figure 1b). However, isolating for values derived from cohesionless substrate (i.e., alluvium; $n=24$), we observe that D increases with precipitation and

Table 1. Reported Values of the Sediment Transport Coefficient D and Associated Crude Climate Data; Includes Brief Descriptions of Vegetation Type and Substrate Material

Study	Site	Climate ^a		Vegetation	Brief Description	D ($\text{m}^2 \text{ka}^{-1}$) ^b
		MAT (°C)	MAP (mm)			
Almond et al. [2008]	Charwell Basin, New Zealand	10.6 ± 3.6	1159 ± 35	Grassland/shrubland Podocarp/beech forest	Fluvial gravel terraces	3.0 ± 1.0
Almond et al. [2008]	Ahuriri, New Zealand	11.8 ± 3.9	662 ± 22	Grassland/shrubland Recent pasture grasses	Thick loess deposits (underlain by altered basalt)	5.0 ± 2.0
Arrowsmith et al. [1998]	Carrizo Plain, CA, USA	14.5 ± 6.2	475 ± 73	Grasses and shrubs	Fault scarp in alluvial gravel	3.1 ± 0.4
Avnac et al. [1993]	Tien Shan, China	9.5 ± 14.2	138 ± 13	Grasses and shrubs	Fault scarp in alluvial gravel	7.0 ± 2.0
Avnac and Peitzer [1993]	Hotan Region, Xinjiang, China	1.8 ± 10.7	33 ± 6	Not vegetated	Fault scarp in alluvial gravel	8.6 ± 0.8
Begin [1992]	Northern Negev, Israel	19.6 ± 5.0	193 ± 36	Not vegetated	Fault scarp in alluvial gravel	5.5 ± 2.0
Bowman and Gerson [1986]	Lake Lisan, Dead Sea	24.3 ± 6.5	142 ± 27	Not vegetated	Fluvial gravel terraces	3.3 ± 1.4
Bowman and Gross [1989] as reported in Hanks [2000]	Northern Arava, Israel	18.8 ± 5.5	198 ± 37	Not vegetated	Lake terraces	0.4 ± 0.3
Carrelier et al. [2002]	Gurvan Bugd fault system, Mongolia	0.3 ± 12.2	160 ± 33	Not vegetated	Fault scarp in alluvial gravel	0.4 ± 0.4
Colman and Watson [1983]	Lake Bonneville, UT, USA	9.5 ± 9.2	456 ± 19	Grasses and shrubs	Alluvial shoreline scarp	3.3 ± 1.7
Constantine et al. [2012]	Simulated Douglas Fir Forest	N/A	N/A	Douglas Fir	N/A	0.1–3.5
Enzel et al. [1996]	Southern Arava Valley, Israel	24.2 ± 6.3	32 ± 6	Not vegetated	Fault scarp in alluvial gravel	0.2–0.3
Gabet [2000]	Transverse Ranges, CA, USA	15.0 ± 4.0	498 ± 83	Coastal Sage	Plio-Pleistocene fanglomerates, Process specific: gopher bioturbation	7.4
Gabet [2003]	Transverse Ranges, CA, USA	15.0 ± 4.0	498 ± 83	Coastal Sage	Plio-Pleistocene fanglomerates, Process specific: dry ravel	0.17
Hanks et al. [1984]	Lake Bonneville, UT, USA	9.5 ± 9.2	456 ± 19	Grasses and shrubs	Alluvial shoreline scarp	1.1
Hanks et al. [1984]	Santa Cruz sea cliffs, CA, USA	13.8 ± 2.8	693 ± 111	Lower terraces are farmed, upper terraces grassland	Quaternary wave-cut terraces cut into Pliocene mudstone	11
Hanks et al. [1984]	Raymond Fault Scarp, LA, CA, USA	18.1 ± 4.2	450 ± 76	Not reported	Fault scarp in alluvial gravel	16
Hanks et al. [1984]	Drum Mtns., UT, USA	10.1 ± 9.9	192 ± 10	Low shrubs (sagebrush and shadscale) 7–20% cover	Fault scarp in alluvial gravel	1.1
Hanks et al. [1984]	Lake Lahontan, NV, USA	10.0 ± 8.5	202 ± 9	Not reported	Alluvial shoreline scarp	1.1
Hanks [2000]	Lost River, ID, USA	3.3 ± 9.1	270 ± 16	Not reported	Fault scarp in alluvial gravel	0.9–1.0
Heimath et al. [2000]	Nummock River, SE Australia	12.8 ± 4.4	827 ± 32	Schlerophyll forest	Soil-mantled granite	4.0
Heimath et al. [2005]	Nunnoch River, SE Australia	12.8 ± 4.4	827 ± 32	Schlerophyll forest	Soil-mantled granite	$D_d = 5.5 \text{ m ka}^{-1}$
Hughes et al. [2009]	Tennessee Valley, CA, USA	13.8 ± 2.8	794 ± 125	Coastal grassland and scrub	Soil-mantled granite	$D_d = 1.25 \text{ m ka}^{-1}$
Hughes et al. [2009]	Point Reyes, CA, USA	12.9 ± 2.9	977 ± 153	Bishop pine forest	Soil-mantled granite	$D_d = 0.5 \text{ m ka}^{-1}$
Hurst et al. [2012]	Charwell Basin, New Zealand	N/A	N/A	Shrubland/grassland (late Pleistocene)	Fluvial gravel terraces (underlain by greywacke)	4.7 ± 2.0
Jungers et al. [2009]	Feather River, CA, USA	10.6 ± 3.6	1159 ± 35	Podocarp and beech forest	Soil-mantled granitoids	8.8 ± 3.0
Martin and Church [1997]	Great Smokey Mountains, NC, USA	13.2 ± 6.5	1508 ± 217	Mixed conifer forest	Soil-mantled quartzite	6.5–10
Nash [1984]	Various	8.4 ± 7.3	1855 ± 24.1	Deciduous forest	From field measurements of volumetric creep rates	0.2
Mattson and Bruhn [2001]	Lake Bonneville, UT, USA	9.5 ± 9.2	456 ± 19	Grasses and shrubs	Alluvial shoreline scarp	1.2 ± 0.3
Mattson and Bruhn [2001]	Wasatch Fault Zone, UT, USA	9.5 ± 9.3	420 ± 17	Not reported	Fault scarp in alluvial gravel	2.8 ± 1.1
McKeen et al. [1993]	East Bay Regional Park, CA, USA	14.9 ± 5.4	522 ± 79	Grasses, clay-rich soil	Soil-mantled Eocene marine shale	36 ± 5
Nash [1980a]	Emmet County, MI, USA	5.7 ± 10.1	825 ± 35	Mixed pine, oak, beech forest	Wave-cut terraces in moraine	12
Nash [1980b]	Drum Mtns., UT, USA	10.1 ± 9.9	192 ± 10	Low shrubs (sagebrush and shadscale) 7–20% cover	Fault scarp in alluvial gravel	0.4
Nash [1984]	Hebgen Lake, MT, USA	1.9 ± 9.6	615 ± 22	Not reported	Fault scarp in alluvial gravel and fluvial gravel terraces	2.0 ± 0.4
Nivière and Marquis [2000]	Upper Rhine Graben, Germany	10.2 ± 6.6	707 ± 32	Forested	Fluvial gravel terraces	1.4
Pellerin et al. [2006]	Lake Bonneville, UT, USA	9.5 ± 9.2	456 ± 19	Grasses and shrubs	Alluvial shoreline scarp	1.0

Table 1. (continued)

Study	Site	Climate ^a		Vegetation	Brief Description	D ($m^2 \text{ ka}^{-1}$) ^b
		MAT (°C)	MAP (mm)			
Pelletier and Cline [2007]	Lathrop Wells, NV, USA	17.6 ± 8.9	109 ± 8	Little vegetation	Lose vesicular scoria lapilli	3.9
Pelletier et al. [2011]	Banco Bonito lava flow, Valles Caldera, NM, USA	4.9 ± 8.4	482 ± 25	Pine, oak, and mixed conifer forest	Soil-mantled rhoylite lava flow	$D = 0.5 \pm 0.2$
Petit et al. [2009]	Wasatch Mtns., UT, USA	8.4 ± 9.3	599 ± 31	Not reported	Soil-mantled gneiss (Precambrian)	$D_d = 0.55 \pm 0.35$
Pierce and Colman [1986]	Big Lost River Valley, ID, USA	5.2 ± 10.0	271 ± 13	Not reported	Alluvial fan scarp	$D = 0.2 \pm 10$
Reneau [1988] reported in Heimath et al. [2005]	Tennessee Valley	13.8 ± 2.8	794 ± 125	Coastal grassland and scrub	Soil-mantled deep marine metasedimentary	5.0
Point Reyes		12.9 ± 2.9	977 ± 153	Bishop pine forest	Soil-mantled granite	3.0
Reneau et al. [1989]	Clearwater River, WA, USA	9.0 ± 4.5	3316 ± 344	Western hemlock and Pacific silver fir forest	Soil-mantled deformed tertiary silts, sandstones, and conglomerates	4.7 ± 2.5
Riggins et al. [2011]	Bodmin Moor, Cornwall, UK	9.2 ± 4.5	1134 ± 52	Grasses, (previous) hazel, and oak woodland	Soil-mantled coarse-grained granite (Permian)	46 ± 16
Roering et al. [1999]	Sullivan Creek, OR, USA	10.8 ± 3.5	1671 ± 205	Douglas fir, mixed conifer forest	Soil-mantled turbidite beds	3.0
Roering et al. [2001b]	Experimental	N/A	N/A		Sand pile disturbed by acoustics	0.27 ± 0.02
Roering et al. [2002]	Charwell River, South Island, New Zealand	10.6 ± 3.6	1159 ± 35	Podocarp and beech forest	Fluvial gravel terraces (underlain by greywacke)	12 ± 8
Roering et al. [2004]	Sullivan Creek, OR, USA	N/A	N/A		Same site as Roering et al. [1999] but post-wildfire	16 ± 6
Roering and Gerber [2005]	Gabilan Mesa, CA, USA	14.7 ± 5.1	278 ± 44	Oak Savannah	Soil-mantled shallow marine and alluvial sediment	11 ± 3.5
Roering et al. [2007]	Santa Cruz, CA, USA	13.5 ± 2.6	713 ± 114	Lower terraces are farmed, upper terraces grassland	Marine terraces cut into Miocene marine mudstone	D in range 38 ± (40/-24) 10
Rosenbloom and Anderson [1994]	Wind River Range, WY, USA	-4.4 ± 7.7	651 ± 13.3	Not vegetated	Soil-mantled crystalline bedrock	17.5 ± 2.7
Small et al. [1999]	Laguna Salada, Baja California, Mexico	21.6 ± 6.3	87 ± 10	Not vegetated	Fault scarps in fluvial gravel terraces	0.051–0.066
Spelz et al. [2008]	Qilian Shan, China	5.9 ± 10.8	137 ± 24	Not vegetated	Fault scarps in Quaternary fanglomerates	3.3 ± 1.7
Tapponier et al. [1990]	Feather River, CA, USA	13.2 ± 6.5	1508 ± 217	Mixed conifer forest	Soil-mantled intermediate metavolcanics	4.8 ± 1.8
This study					Soil-mantled granodiorite	8.8 ± 3.3
Walther et al. [2009]	Blue Mountains, WA, USA	-0.7 ± 15.6	305 ± 60	Coniferous forest	Soil-mantled basalt	4.8 ± 0.7

^aMean annual temperature (MAT) and mean annual precipitation (MAP) calculated over the period 1950–2000. Data from the WorldClim global climate 30 arc-second dataset (<http://www.worldclim.org>; accessed 6 August 2011) (Hijmans et al., 2005). Error ranges are 1σ of monthly means as an indicator of seasonality.

^bWe report absolute values, range constraints, and/or error estimates as they appear in the literature.

^cPierce and Colman [1986] found that D ranged over two orders of magnitude depending on the scarp aspect.

^dLarge range due to poor constraints on boundary erosion rate.

seasonality (Figures 1b and 1c; seasonality defined here as the standard deviation about mean annual precipitation), as suggested by *Hanks* [2000]. Yet it seems likely that both substrate lithology and climate will control D , since lithology will influence the production and material properties of the soil, and climate will control the style and efficiency of processes which mobilize the soil. If lithology can significantly influence hillslope sediment transport, we anticipate differences in landscape morphology for adjacent areas (with similar climate) overlying distinct bedrock types, even if the mechanisms of sediment transport are similar.

[6] In soil-mantled, forested landscapes, the dominant mechanism of sediment flux is often via tree throw, and the growth and decay of tree roots [e.g., *Roering et al.*, 2010; *Gabet and Mudd*, 2010; *Constantine et al.*, 2012]. The efficiency of sediment transport may therefore be strongly linked to the amount and type of vegetation acting to disturb sediment. *Hughes et al.* [2009] inferred that sediment transport increased at the start of the Holocene due to colonization by forests, replacing previous grassland in the Charwell Basin, New Zealand (Table 1). Light Detection and Ranging (LiDAR) allows for quantification of metrics for aboveground biomass, such as vegetation density or mean canopy height [e.g., *Nilsson*, 1996; *Naesset*, 1997; *Lefsky et al.*, 2002; *Holmgren et al.*, 2003; *Donoghue and Watt*, 2006], which can be compared to topographic attributes to explore whether D may vary systematically as a function of vegetation [*Pelletier et al.*, 2011].

[7] The morphology of soil-mantled hillslopes reflects the processes which create and redistribute sediment downslope, and the erosion rate in the adjacent channels. Where constraints have been placed on erosion rates within a landscape, one may infer the nature of sediment transport based on the morphological properties of hillslopes such as hilltop curvature C_{HT} , mean hillslope gradient S , and hillslope length L_H [e.g., *Roering et al.*, 2007; *Roering*, 2008; *Hurst et al.*, 2012]. In this contribution, we extract these properties from high resolution (1 m grid) topography, derived from airborne LiDAR, to compare the topographic signature of landscapes in two distinct lithologies, the granodiorite of the Cascade pluton and the metavolcanic rocks of the Central Belt in the northern Sierra Nevada of California. In this region, we have constraints on rock uplift rates and associated transient erosion rates [*Riebe et al.*, 2000; *Wakabayashi and Sawyer*, 2001; *Hurst et al.*, 2012], present day climate, and current vegetation. Hence, there is an opportunity to quantitatively analyze the morphological properties of rapidly denuding, soil-mantled hillslopes in two distinct lithologies in order to investigate the control bedrock type plays in a soil-mantled landscape. We sought to quantify the efficiency of sediment transport processes on hillslopes in two distinct lithologies and identify whether any differences could be attributed to climate, the type and distribution of vegetation, or underlying lithology. We investigated differences in the distribution of hillslope gradients between bedrock types. Finally, we documented differences in the length of hillslopes between the two lithologies, and a tendency for hillslope lengths to shorten with increasing erosion rate, suggesting that drainage density may be controlled by erosion rate.

2. Theory on Hillslope Morphology

2.1. Hillslope Mass Balance and Sediment Transport Equations

[8] The spatial and temporal evolution of soil-mantled landscapes can be examined using principles of mass conservation [Gilbert, 1909; Culling, 1960; Dietrich et al., 2003] where the surface elevation ζ [L] changes in time t relative to a moving reference elevation ζ_0 [L] [e.g., *Mudd and Furbish*, 2005]. The surface elevation evolves according to the following:

$$\frac{d\zeta}{dt} = -\frac{d\zeta_0}{dt} \nabla q_s, \quad (1)$$

where q_s [$L^2 T^{-1}$] is the volumetric sediment flux per unit contour width. We equate the lowering rate of the reference elevation ζ_0 to the rate of local bedrock lowering (i.e., valley incision) at the base of the hillslope (E [$L T^{-1}$]) such that $d\zeta_0/dt = -(\rho_t / \rho_s)E$ where ρ_t and ρ_s [$M L^{-3}$] are the densities of bedrock and dry soil, respectively. If the entire hillslope lowers at the same rate as the channel, then equation (1) reduces to

$$\frac{\rho_t}{\rho_s} E = \nabla q_s. \quad (2)$$

[9] Equations (1) and (2) assume that all mass transport is the result of physical processes, and mass/volume change due to aeolian processes is negligible. We do not account for volume changes in soils due to chemical denudation. *Riebe et al.* [2001] demonstrated that chemical denudation scales with total denudation in granitoid portions of our study area and that chemical denudation is small compared to physical denudation and should have minimal impact on hillslope morphology [e.g., *Mudd and Furbish*, 2004].

[10] Most processes which act to transport sediment down a hillslope are gravity driven and are therefore dependent on hillslope angle; both grain displacements during disturbance (normal to the surface) and subsequent gravitational settling (vertical) increase with steeper slopes [e.g., *Roering et al.*, 1999; *Furbish et al.*, 2009]. On gentle, soil-mantled hillslopes, sediment flux, q_s , is often attributed to slope-dependent creep-like processes [Davis, 1892; Gilbert 1909]. However, in landscapes with high relief, hillslopes often become planar away from topographic divides, commonly inferred to be driven by a process transition to landslide-dominated sediment flux [e.g., *Howard*, 1994; *Roering et al.*, 1999; *Binnie et al.*, 2007] and/or an increase in particle displacement distances [e.g., *Tucker and Bradley*, 2010; *Foufoula-Georgiou et al.*, 2010]. *Roering et al.* [1999] formulated a disturbance-driven transport law allowing sediment flux to increase in a non-linear fashion with hillslope gradient to account for this process transition. As local gradient approaches a critical slope S_C , which field studies have shown to vary between 0.8 [DiBiase et al., 2010; *Hurst et al.*, 2012] and 1.25 [*Roering et al.*, 1999], sediment flux asymptotically approaches infinity [Andrews and Bucknam, 1987; *Anderson*, 1994; *Roering et al.*, 1999]:

$$q_s = -D \nabla \zeta \left[1 - \left(\frac{\nabla \zeta}{S_C} \right)^2 \right]^{-1}, \quad (3)$$

where D [$L^2 T^{-1}$] is a transport coefficient. Equation (3) has empirical and experimental support [*Gabet*, 2000; *Roering*

et al., 2001a; *Pelletier and Cline*, 2007]. We do not consider similar depth-dependent models [e.g., *Heimsath et al.*, 2005] since soil depth does not vary systematically with erosion rate in the soil-mantled portions of our field site [*Yoo et al.*, 2011], and we restrict our analyses to the soil-mantled areas of the field site.

[11] In Equation (3), the combined influences of climate and lithology on a suite of processes are lumped into a single parameter, D . These processes include freeze/thaw, wet/dry, and shrink/swell cycles [*Gilbert*, 1909]; bioturbation due to tree throw [e.g., *Roering et al.*, 2010; *Gabet and Mudd*, 2010; *Constantine et al.*, 2012] or burrowing organisms [*Gabet*, 2000; *Yoo et al.*, 2005]; and rainsplash grain displacement [e.g., *Dunne et al.*, 2010]. *Hanks* [2000] documented that D increases systematically with climate from $D = 0.1\text{--}0.7 \text{ m}^2 \text{ ka}^{-1}$ in the arid Middle East [*Bowman and Gerson*, 1986; *Bowman and Gross*, 1989; *Begin* 1992] through $0.5\text{--}2.0 \text{ m}^2 \text{ ka}^{-1}$ and $3.3\text{--}5.5 \text{ m}^2 \text{ ka}^{-1}$ in the semi-arid regions of the western U.S. [*Hanks et al.*, 1984; *Hanks and Wallace*, 1985; *Hanks and Andrews*, 1989; *Hanks*, 2000] and western China [*Tapponier et al.*, 1990; *Avouac et al.*, 1993; *Avouac and Peltzer*, 1993], respectively, to $8.5\text{--}16 \text{ m}^2 \text{ ka}^{-1}$ in more humid coastal California [*Hanks et al.*, 1984; *Arrowsmith et al.*, 1998] and Michigan [*Nash*, 1980a]. Several studies have postulated increased hillslope sediment transport rates at the glacial-interglacial transition between the late Pleistocene and early Holocene in New Zealand, attributed to changes in vegetation density and type [*Roering et al.*, 2004; *Almond et al.*, 2008; *Hughes et al.*, 2009; *Walther et al.*, 2009]. Variation in the type and density of vegetation may also occur as soil conditions, and the availability of nutrients changes at lithologic boundaries.

2.2. Hillslope Morphology

[12] When hillslope gradient ($\nabla\zeta$) is small, the bracketed term in equation (3) approaches unity. Substituting equation (3) into equation (2), we can therefore solve for erosion rate where slope angles are low (i.e., on hilltops):

$$E = -\frac{\rho_s}{\rho_r} DC_{\text{HT}}, \quad (4)$$

where C_{HT} is the hillslope curvature, i.e., $\nabla^2\zeta$, at the hilltop, since this is where we expect hillslope gradients to be the gentlest. Equation (4) predicts that the erosion rate on a steadily denuding hillslope should be linearly proportional to hilltop curvature C_{HT} and the sediment transport coefficient D . We adopt the sign convention that convex up surfaces (i.e., hilltops) have negative curvature and erosion is a positive quantity (i.e., a positive value of E indicates a lowering of the land surface). Equation (4) predicts erosion rates as a function of hillslope topography as long as $(\nabla\zeta/S_C)^2$ in equation (3) is small enough to be negligible. Equation (3) describes hillslope sediment transport; in valleys, fluvial transport and erosion dominate. Thus, equation (3) applies to the convex portions of the landscape [e.g., *Roering et al.*, 2007]. The lowest gradients within the convex portions of the landscape, where equation (3) is most likely to occur, are on hilltops. Critically, however, this relationship *only* applies when the hilltop has attained topographic steady state; that is to say the rate of denudation should be the same everywhere on the hillslope, matching the rate in the channel at the base of the hillslope. During landscape adjustment to

tectonics and/or baselevel change, hilltops are always the last part of the landscape to respond [e.g., *Furbish and Fagherazzi*, 2001; *Mudd and Furbish*, 2007].

[13] Hillslope relief has also been used to estimate erosion rates, but once erosion rates exceed $\sim 100\text{--}300 \text{ mm ka}^{-1}$, further increases in erosion rates are accommodated by increased landsliding frequency on threshold slopes and hillslope gradients or hillslope relief become poor predictors of erosion rates [e.g., *Burbank et al.*, 1996; *Binnie et al.*, 2007; *Ouimet et al.*, 2009; *DiBiase et al.*, 2010; *Larsen and Montgomery*, 2012]. Equation (4) provides an alternative approach to estimating erosion rates from topography in landscapes with steep, planar hillslopes [*Hurst et al.*, 2012]. *Roering et al.* [2007] provided a comprehensive framework for analyzing relationships between denudation and hillslope topography (i.e., relief, topographic slope, curvature, and hillslope length) when equation (3) is combined with the mass balance equation (equation (2)) in 1D form. Non-dimensionalization of erosion rate and relief allows comparisons between landscapes with distinct process rates and morphology. *Roering et al.* [2007] cast erosion rate and relief in non-dimensional form (E^* and R^* , respectively) as functions of topographic parameters C_{HT} , L_H , and mean hillslope gradient S :

$$E^* = \frac{E}{E_R} = \frac{\rho_r}{\rho_s} \frac{2EL_H}{DS_C}. \quad (5a)$$

$$E^* = \frac{2C_{\text{HT}}L_H}{S_C}. \quad (5b)$$

$$R^* = \frac{1}{E^*} \left\{ \sqrt{1 + (E^*)^2} - \ln \left[\frac{1}{2} \left(1 + \sqrt{1 + (E^*)^2} \right) \right] - 1 \right\}. \quad (6a)$$

$$R^* = \frac{S}{S_C}. \quad (6b)$$

[14] Equation (6a) predicts a non-linear relationship between E^* and R^* , which all hillslopes with a morphology that is adjusted to its boundary conditions should obey (provided that equation (3) gives a reasonable approximation of sediment transport processes on the hillslope). Similarly to equation (3), the prediction of equation (6a) only holds when the hillslope is denuding in concert with the adjacent channel. However, equations (5b) and (6b) allow us to calculate E^* and R^* from topographic attributes, even where the steady state assumption is violated, in order to compare to the model predictions for steady state encapsulated in equation (6a). In such a scenario, hillslope morphology is expected to vary from the model prediction in a manner that reflects the style of transience [*Hurst et al.*, 2012]. We therefore developed techniques to quantify the spatial distribution of C_{HT} , L_H , and S within a landscape from LiDAR-derived topography in order to explore the spatial distribution of E^* and R^* and their relationship to bedrock type.

3. Methods

3.1. Quantifying Hillslope Morphology

[15] In forested landscapes, high resolution LiDAR DEMs commonly exhibit high local variability due to the presence of pits associated with the upheaval or decay of tree root clumps [e.g., *Roering et al.*, 2010] or dense vegetation or

"brush" which has been misclassified as bare earth [Lashermes *et al.*, 2007]. Thus, standard algorithms computing slope and curvature from 3×3 pixel moving windows produce noisy results. Assuming a diffusion-like model for sediment transport requires slope to be calculated at a larger scale than that at which the disturbance forces operate [Joytsna and Haff, 1997; Furbish *et al.* 2009]. Lashermes *et al.* [2007] found that a length scale (where length scale is twice the search radius) of 12 m was appropriate for LiDAR from the South Fork Eel River, CA, whilst Roering *et al.* [2010] demonstrated a length scale of 15 m in the forested landscape of the Oregon Coast Range. At our field site, the appropriate scaling was 12 m [Hurst *et al.*, 2012]. Here we calculated the slope, curvature, and aspect from a 6-term quadratic surface fitted to a 12×12 m window in the gridded elevation data, centered on the pixel of interest [see Hurst *et al.*, 2012].

[16] A hillslope can be considered to begin at a topographic divide and extend to a valley bottom, at which a transition from hillslope processes (i.e., diffusive processes and landslides) to valley-forming processes occurs (i.e., debris flow and/or fluvial erosion). We extracted hilltops from the LiDAR DEM as the intersecting margins of zero-order and upward drainage basins, where slope ($\nabla \zeta$) < 0.4 . The valley network was defined using the Geonet algorithm of Passalacqua *et al.* [2010]. Hilltop curvature C_{HT} was sampled at all pixels within 2 m of these hilltops. Adjacent hillslopes were sampled using an aspect-driven routing algorithm [Lea, 1992] to trace from each hilltop pixel to an adjacent valley bottom. Along the resulting profile, the mean slope (S), relief (R), and horizontal hillslope length (L_H) were recorded. A mean value for each of these metrics was then determined for each hilltop segment [see Hurst *et al.*, 2012, for detailed description of methods].

3.2. Quantifying Vegetation Properties

[17] Sediment transport in forested, soil-mantled landscapes is driven, in part, by tree turnover through growth and decay of tree roots and the upheaval of tree root wads [e.g., Schatzel and Follmer, 1990; Gabet *et al.*, 2003; Gabet and Mudd, 2010]. Therefore, it has been suggested that the sediment transport coefficient (D in equation (3)) may vary with aboveground biomass (AGB) [Roering *et al.*, 2004; Walther *et al.* 2009]. Airborne-derived LiDAR data collected from forested landscapes contain a wealth of information about vegetation, with last/lowest returns being generally classified as the ground surface and all aboveground returns being reflected from vegetation surfaces (leaves, branches, etc.). Properties of the canopy elevation structure such as the mean and standard deviation of the height of canopy returns (V_{mean} and V_{sd} , respectively) can be readily extracted from LiDAR [e.g., Nilsson, 1996; Naesset, 1997; Lefsky *et al.*, 2002; Holmgren *et al.*, 2003; Donoghue and Watt, 2006] and may provide useful indicators of AGB [e.g., Hall *et al.*, 2005; Clark *et al.* 2011; Pelletier *et al.*, 2011; Saatchi *et al.*, 2011]. Clark *et al.* [2011] found that LiDAR-derived metrics V_{mean} and V_{max} provided robust indicators of measured AGB. Pelletier *et al.* [2011] used a 1 m resolution canopy height map derived from LiDAR to demonstrate a negative relationship between mean C_{HT} and V_{mean} , suggesting that vegetation cover may be controlling the sediment transport coefficient D .

[18] Here we investigated how vegetation cover varies on hilltops as a function of lithology between the two study areas to assess whether variation in quantifiable vegetation metrics derived from LiDAR could account for differences in the efficacy of sediment transport. The approach is limited by the assumption that modern vegetation accounts for the current shape of hillslopes, yet others have attributed change in biologically driven sediment transport to change in vegetation cover at the end of the last glaciation [e.g., Roering *et al.*, 2004; Walther *et al.*, 2009].

[19] We analyzed point cloud density and height above the ground surface for returns classified as vegetation. Return classification was carried out by the National Center for Airborne Laser Mapping. To estimate canopy height, the heights of aboveground point returns were detrended by subtracting the elevation of the ground surface interpolated to a 1 m grid. The resulting canopy heights were analyzed to compute values for V_{mean} and V_{sd} in each grid cell in 4 m resolution grids (coarsened to avoid data gaps where there were no aboveground LiDAR returns). Although the low-relief portions of the landscape have been heavily logged, there is no evidence of recent logging (i.e., no cut stumps and numerous trees with diameters exceeding 1 m). Canopy height data from the LiDAR appear to qualitatively agree with satellite imagery (i.e., bare patches apparent on satellite images correspond to absent or minimal canopies from LiDAR). We defined a vegetation density ratio V_{dens} as the ratio between the points classified as aboveground and points classified as ground, normalized to the total number of returns within a 4 m resolution grid. A ratio $V_{\text{dens}} = 1$ indicates that all points returned were aboveground and the canopy is dense, whilst a ratio $V_{\text{dens}} \rightarrow 0$ indicates little/no vegetation cover. We consider this a crude approach since the results are limited by the average point spacing of LiDAR returns ($\sim 4 \text{ m}^{-2}$) and may be influenced by any variation in leaf structure and tree spacing.

4. Study Sites

[20] We explored hillslope morphology in the lower reaches of the Middle Fork Feather River, in the northern Sierra Nevada of California (Figure 2). Our study is focused on an area where granitoid plutons are intruded into the Central belt terrain which consists of Upper Triassic-Jurassic ophiolitic, volcanic, and sedimentary units of the Fiddle Creek Complex [Day and Bickford, 2004] (Figure 3).

[21] The landscape comprises a low-relief, relict surface characterized by concave up channel profiles and broad "diffusive" hillslopes which is likely adjusted to some previous erosional regime. This landscape is dissected by the canyons of the Middle Fork Feather River and its tributaries (Figure 2). Canyon incision was initiated by accelerated uplift c. 3.5–5 Ma [Wakabayashi and Sawyer, 2001; Stock *et al.*, 2004], possibly caused by the delamination of an eclogite root beneath the mountain range [Saleeby and Foster, 2004; Jones *et al.*, 2004]. Apatite fission track dates reveal an average erosion rate of 40 mm ka^{-1} for the relict landscape, persisting until at least 32 million years ago (Ma) [Cecil *et al.*, 2006]. Long-term exhumation rates derived from (U-Th)/He ages fail to record a late-Cenozoic acceleration in denudation, implying that less than 3 km of the crust has been exhumed since the acceleration

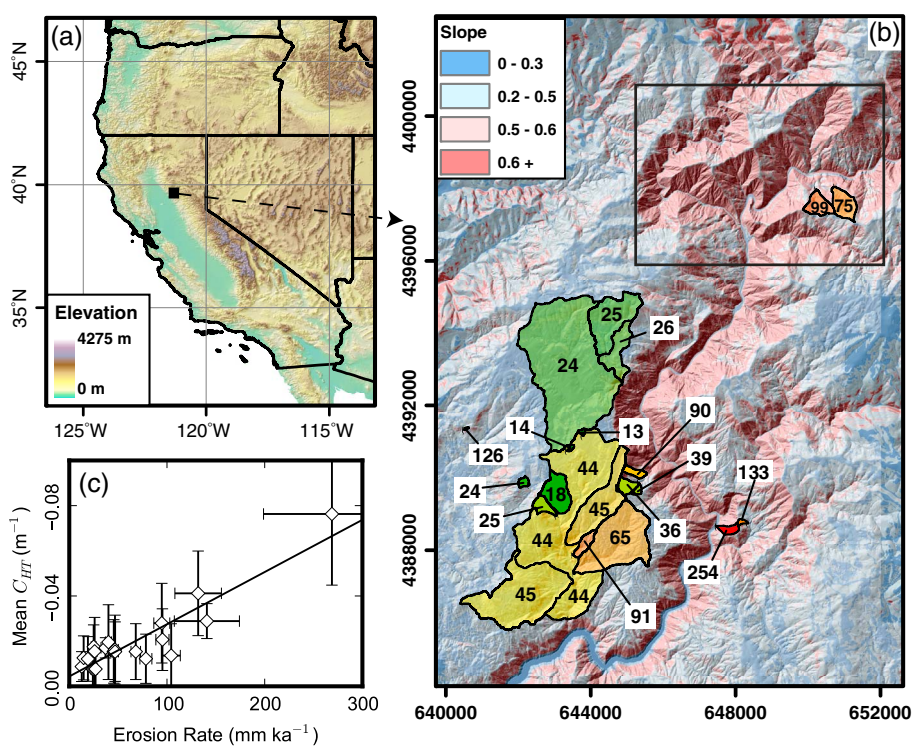


Figure 2. (a) Location of study area in Sierra Nevada of northern California. (b) High resolution (LiDAR) shaded slope map of the study area along the Feather River (Middle Fork); low gradients are blue; steep slopes are red. Overlain are CRN sample sites with estimated basin-averaged erosion rates in mm ka^{-1} (shaded green to red with increasing erosion rate, uncertainties on these estimates are shown in (c)) [Hurst et al., 2012]. Samples were taken for basins exclusively in granitoid bedrock. Erosion rates vary over an order of magnitude from the canyon to the adjacent relict upland. (c) Plot of mean hilltop curvature compared to denudation rate in each of the basins sampled. Solid line represents a linear relationship between hilltop curvature and denudation ($R^2=0.83$), as predicted by equation (4), allowing the sediment transport coefficient to be constrained at $8.6 \text{ m}^2 \text{ ka}^{-1}$ [see Hurst et al., 2012]. The black box shows the location of Figure 3. The spatial reference system is UTM Zone 10N with spatial units in meters.

[Cecil et al., 2006]. Incision rates for the Feather River canyon have been reconstructed for the last 5 Ma from the presence of late-Cenozoic volcanics capping ridges/divides with the Feather River having an estimated minimum incision rate of 170 mm ka^{-1} over the last 5 Ma [Wakabayashi and Sawyer, 2001]. Erosion rates measured within the Feather River basin vary by over an order of magnitude from the relict surface ($\sim 20 \text{ mm ka}^{-1}$) to the canyons ($\sim 250 \text{ mm ka}^{-1}$) [Riebe et al., 2000; Wakabayashi and Sawyer, 2001; Hurst et al., 2012] (Figure 2b). For several catchments $>200 \text{ km}$ south of the Feather River, Stock et al. [2004] established canyon erosion rates of $\sim 200 \text{ mm ka}^{-1}$ between 1.5 and 2.7 Ma, compared with $\sim 30 \text{ mm ka}^{-1}$ since 1.5 Ma, from CRN dating of cave sediments now suspended above the valley floor. They attributed this change to an incision wave propagating upstream 2–5 Ma ago due to accelerated tectonic uplift.

[22] The modern climate is semi-arid with a strong precipitation gradient from the dry Central Valley of California to the high elevations of the Sierra Nevada mountains. At our study site, mean annual temperature is 12.5°C and mean annual precipitation is 1750 mm (data from the PRISM Climate Group, Oregon State University, <http://prism.oregonstate.edu> (accessed 7 July 2011) [Daly et al., 1997]). The Feather River basin remained largely unglaciated during the Pleistocene,

except for its uppermost reaches [Wahrhaftig and Birman, 1965; Clark, 1995].

[23] Hurst et al. [2012] extended the dataset used by Riebe et al. [2000] and demonstrated that as basin-averaged erosion rates increase, hilltops get sharper (i.e., curvature becomes more negative) in granitoid portions of the landscape (Figure 2c). A linear relationship provides the best fit ($R^2=0.83$), but Hurst et al. [2012] could not rule out the possibility of an exponential relationship ($R^2=0.72$). Mean slope angles vary non-linearly with erosion rate, suggesting that some hillslopes in the field area approach the critical gradient (i.e., S_C), and thus, their mean gradient may be insensitive to increases in erosion rate. Hillslope gradients rarely exceed 0.9, and there is evidence of landsliding in the steepest parts of the landscape. This is consistent with a sediment transport law in which flux increases to infinity as slopes approach some limiting angle (approximating the effect of increased landslide frequency), as in equation (3), as previously demonstrated in other landscapes [e.g., Binnie et al., 2007; Ouimet et al., 2009; DiBiase et al., 2010].

[24] We focused our analysis on the area near the confluences of the Little North Fork and Cascade Rivers with the Feather River (Figure 3). In the east of the area shown in Figure 3, the bedrock is the granodiorite of the Cascade Pluton; in the west, intermediate volcanics of the Fiddle Creek

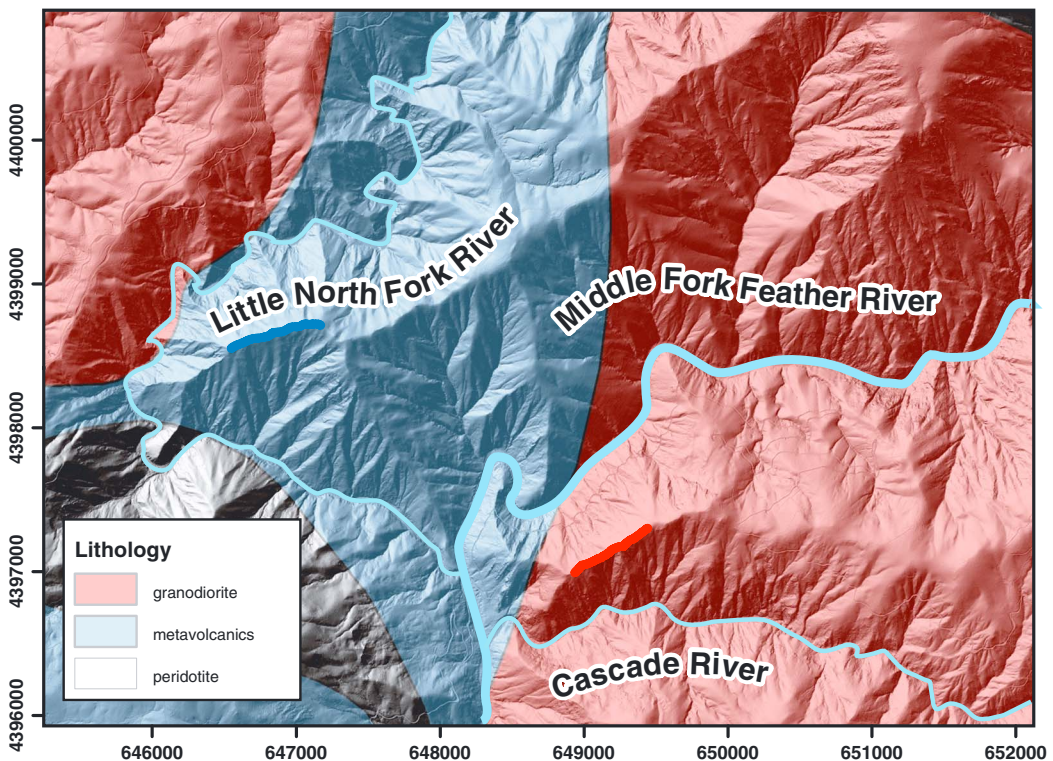


Figure 3. Shaded relief image of study site with lithology superimposed [Moosdorff et al., 2010]. Topographic metrics from all hillslopes in granodiorite in the east and metavolcanics to the west were retrieved, with more detailed analysis focused on the two ridge transects highlighted in red and blue, respectively. The principle drainage conduits are highlighted in light blue. The spatial reference system is UTM Zone 10N with spatial units in meters.

complex. With the Feather River downcutting rapidly, the Little North Fork and Cascade rivers are undergoing a transient adjustment to acceleration in baselevel lowering. We studied hilltops and adjacent hillslopes near the confluences where they were most likely to be adjusting/adjusted to baselevel lowering, since adjacent valleys are downstream of major knickpoints (location of a sudden increase in slope downstream; Figure 4). The studied hillslopes, separated by less than 5 km and spanning similar ranges in elevation, can be assumed to have similar climatic histories, and their proximity to the Feather River implies similar denudation history. Based on field observations, a significant driver of sediment transport in this forested landscape is growth/decay of tree roots and the upheaval of root wads and associated soil by tree throw. Thick soils are developed on steep slopes in both areas (Figure 5). The two areas lie in the Plumas National Forest, and vegetation consists of the California mixed conifer forest type, which includes Douglas fir, incense-cedar, and sugar pine [Warbington and Beardsley, 2002].

5. Results

5.1. Morphology of Hillslopes as a Function of Lithology

[25] Figure 6 shows the spatial distribution of hilltops sampled and their hilltop curvature. The highest values of hilltop curvature (i.e., the most convex or sharpest hilltops) occur on hilltops most proximal to the Feather River, the Cascade River, and the Little North Fork River, downstream

of the main knickpoints (Figure 4). High values of hilltop curvature are spatially more distributed in the northwest of the study area since the knickpoint has propagated further up the Little North Fork tributary than along Cascade River. In Figure 7, the relationship between hilltop curvature and hillslope gradient is compared for the granodiorite and metavolcanics. We find a non-linear relationship between mean hilltop curvature and mean hillslope gradient. Where there is low hilltop curvature, hillslope gradients are also low. As hilltop curvature increases, so too does hillslope gradient; however, beyond $C_{HT} \sim -0.03 \text{ m}^{-1}$ (i.e., where C_{HT} is more negative), hillslope gradients do not continue to increase as rapidly. This relationship occurs in both lithologies, but the two datasets are offset such that in the metavolcanics, for low values of hilltop curvature (greater than -0.03 m^{-1}), hillslopes tend to be steeper, and hillslopes in the metavolcanics approach their limiting gradient at lower hilltop curvatures than in the granodiorite. Since hillslope gradients appear to be limited, they will not reflect the erosion rates driving their evolution; however, following equation (4), hilltop curvature may better reflect the distribution of erosion rates if the hillslope has fully responded to the change in boundary conditions [Hurst et al., 2012].

[26] We cast these results in non-dimensional form to compare them to the expected form of model hillslopes governed by equation (3), calculating dimensionless erosion rate as a function of hilltop curvature and hillslope length, and dimensionless relief as a function of mean slope (equations (5b) and (6b)) [Roering et al., 2007]. Despite considerable scatter,

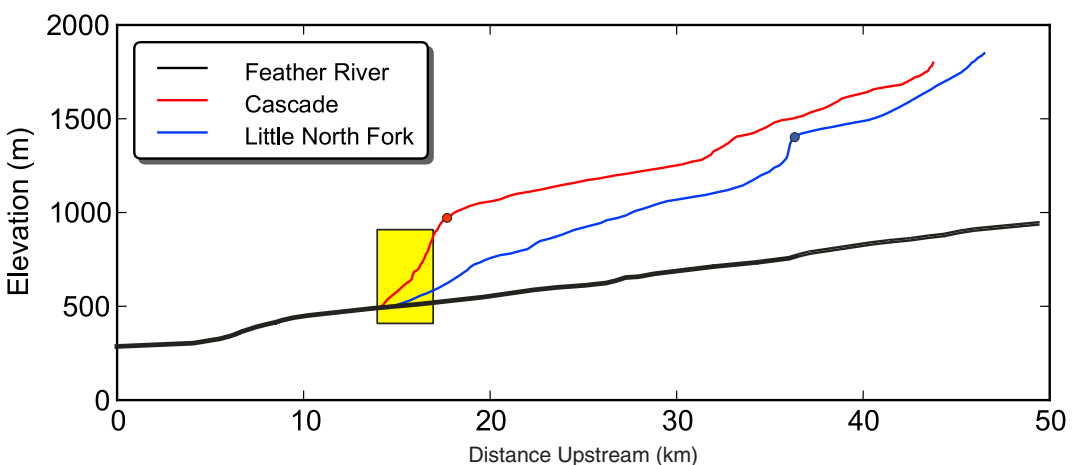


Figure 4. Longitudinal profiles for Little North Fork (blue) and Cascade (red) rivers relative to the lower reaches of the Feather River (black) which sets baselevel. Profiles were generated from U.S. Geological Survey National Elevation Dataset 1/3 arc-second (approx. 10 m) DEMs [<http://seamless.usgs.gov/>; accessed 15/1/2009]. Shaded region indicates area in which the landscape is interpreted to be adjusting or adjusted to the rapid incision rate of the Feather River along both the Little North Fork and Cascade Rivers, downstream of major knickpoints marked with filled circles. Note these knickpoints both fall out with the bounding region of Figure 3. The lower reaches of Cascade and Little North Fork rivers cross the Cascade Pluton (granodiorite) and Central Belt (metavolcanics), respectively.

we found that the distribution of binned R^* and E^* is of a similar form to that predicted by equation (6a), as depicted by the dashed line in Figure 8. Note from equations (5b) and (6b) that S_C is required to quantify both E^* and R^* based on measurable topographic properties, and hence, the value of S_C used can alter the position of the data relative to the dashed steady state line (see section 5.2). E^* was calculated as a function of hilltop curvature and hillslope length (equation (5b)). Despite non-dimensionalization, there is still a tendency for

hillslopes in the metavolcanics to be steeper when E^* is low. Frequency distributions of hillslope lengths (Figure 9a) reveal that hillslopes are slightly longer in the metavolcanics (peak at 175–200 m, and a larger proportion of long hillslopes) than in the granodiorite (peak at 150–175 m, with a larger number of short hillslopes). We carried out a *t*-test to test the equality of the two sample means and concluded at 99% confidence that the samples were drawn from different populations. This is also shown by plotting C_{HT} (controlled by E) versus L_H



Figure 5. Example soil pits in (left) granodiorite and (right) metavolcanics. Pit in granodiorite comes from hilltop along cascade ridge (red line in Figure 4) with hilltop curvature $C_{HT} = -0.062$; pit depth is 65 cm. Pit in metavolcanics on steep slope (c. 40°) on the western flank of the Little North Fork River; pit depth is 85 cm.

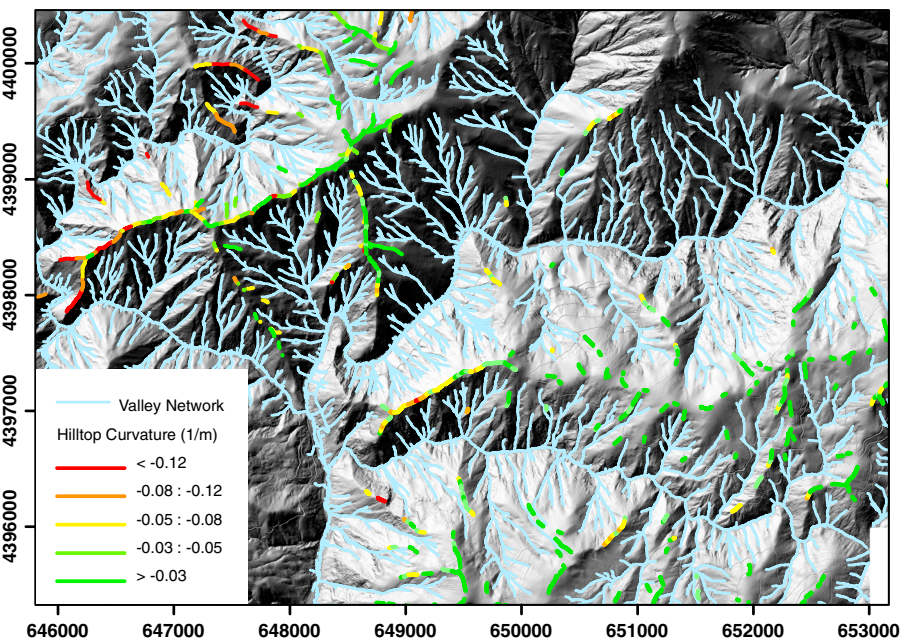


Figure 6. Map of channel and hilltop networks in the study region. Hilltops are color coded by hilltop curvature, with the highest values of hilltop curvature occurring mainly in the metavolcanics and adjacent to the main drainage routes. Channel network extracted using the Geonet tool [Passalacqua et al., 2010]; hilltops defined as the adjoining edges of drainage basins extracted at all stream orders (see text).

(Figure 9b), which indicates that hillslope lengths have a tendency to shorten in response to increased erosion rates (as signified by increased C_{HT}). The tendency of hillslopes to be steeper in the metavolcanics is therefore not the result of hillslopes being longer (and consequently having a larger proportion of their length that is steep and planar), since non-dimensionalizing normalizes for hillslope length. The tendency for hillslopes to be steeper in the metavolcanics may relate to a difference in the limited slope angle that hillslopes can attain in the two lithologies, or to differences in the transient development of the hillslopes in response to baselevel fall. Hillslopes with high hillslope gradient but low hilltop curvature (or high R^* but low E^*) are expected to develop when a hillslope is adjusting to an increase in erosion rate, or the passing of a knickpoint at its toe [Hurst et al., 2012]. Hillslopes in metavolcanics tend to be steeper than in granodiorite for similar values of C_{HT} which might suggest there are more transient hillslopes in the metavolcanics.

5.2. Constraining S_C

[27] Critical slope S_C is used when calculating both E^* and R^* from topographic metrics. We estimated S_C by finding the maximum likelihood estimator (MLE) between the hillslope data and model predictions for R^* as a function of E^* (equation (6a)) with varying S_C . It is important to highlight here that the model fitted applies to steady state hillslope morphology, yet the landscape analyzed spans a range of erosion rates (Figure 2) and there are knickpoints in the channel system (Figure 4). Thus, it is likely that some hillslopes may have transient morphology. Nevertheless, the tendency of the asymptote created by equation (6a) (see dashed line in Figure 8) is controlled by S_C , and the highest values of R^* contained in the datasets should reflect S_C . The MLE was calculated as follows, reporting error

range at one standard deviation of the normalized probability distribution:

$$MLE = \prod_{i=1}^n \exp \left[\frac{(R^*_{\text{meas}} - R^*_{\text{mod}})^2}{2\sigma_p} \right], \quad (7)$$

where n is the number of hillslopes sampled, the subscripts meas and mod refer to measured and modeled values, respectively, and σ_p is the variance in measured R^* values, which will alter the magnitude of MLE calculated but will not change the most likely value of S_C . The MLE for S_C was $0.79 - 0.07/ +0.38$ for the granodiorite and $0.85 - 0.08/+0.53$ for the metavolcanics. This indicates that the maximum attainable gradient on hillslopes in the metavolcanics may be slightly higher. We interpret the large range in error values as due to a significant proportion of hillslope data having low E^* (<10) and R^* (<0.8) (Figure 8), at which the model predictions are insensitive to changes in S_C . Having more data points at high E^* would significantly reduce the error range since it is at high erosion rates that hillslopes become steep and planar and are most likely to reflect S_C . The likelihood that S_C is 0.85 and 0.79 in the granodiorite and metavolcanics (i.e., that our result is reversed) is over a factor of two less likely. As hillslopes become steep and planar, mean hillslope gradient S should approach S_C . Mean hillslope gradients presented in Figure 7 rarely exceed 0.8, suggesting that the values calculated here are appropriate; however, we also note that we were unable to demonstrate a statistical difference in S between the two lithologies at high C_{HT} , which might otherwise have corroborated our calibrated values.

[28] Slope histograms were computed for hillslope areas nearest to the tributary junctions with the Feather River, i.e., the parts of the landscape with the steepest slope. We avoided sampling where there were obvious remnants of the relict upland, concentrating instead on hillslopes adjacent to

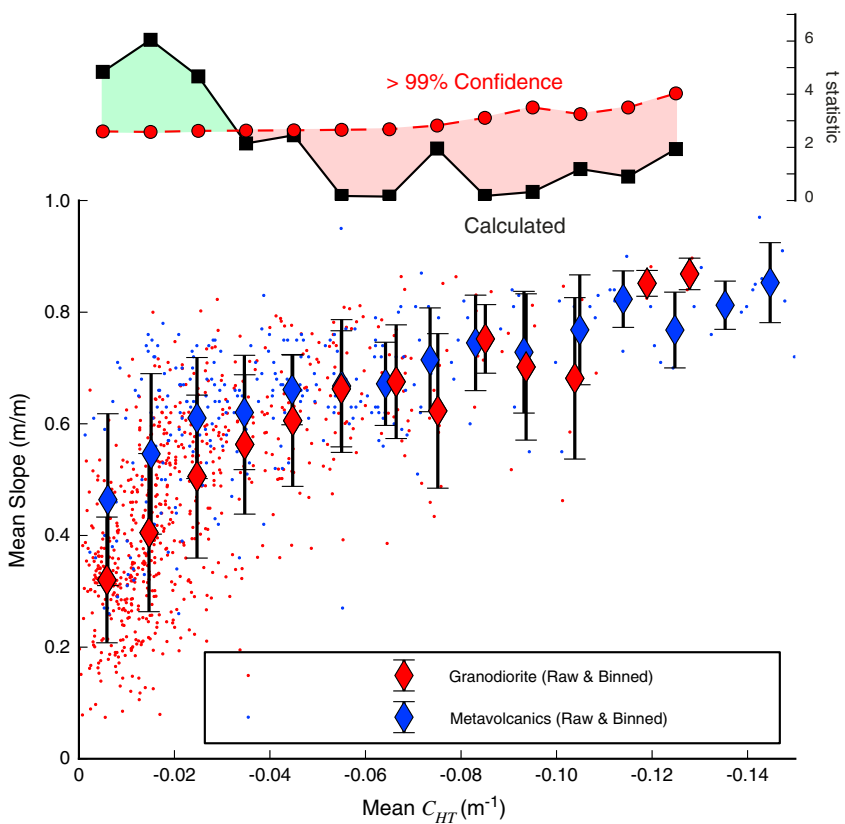


Figure 7. Relationship between mean hilltop curvature (C_{HT}) and mean adjacent slope (S) for hilltops in the granodiorite (red) and metavolcanics (blue), with Students t -statistic used to compare between the two datasets. Where the calculated t -statistic (black) falls above the 99% confidence level (red dashed), the two datasets can be interpreted as originating from different populations (area shaded green). Data are binned into regularly spaced bins in C_{HT} . C_{HT} is expected to be a good indicator of relative erosion rate, whilst at high erosion rates, S becomes insensitive to baselevel fall. Note we plot bin-mean averaged C_{HT} and S . In both lithologies, C_{HT} continues to vary despite S becoming limited. For low C_{HT} , hillslopes are steeper in the metavolcanics (at 99% confidence level). S in both lithologies appears to be limited to ~ 0.85 .

canyons. Figure 10 shows slope histograms sampled for both granodiorite and metavolcanics portions of the landscape which are downstream of convexities in the channel profile. The two lithologies have similar mean (0.84 and 0.85) and median (0.83 and 0.86) slope values for granodiorite and metavolcanics, respectively.

5.3. Estimates of Aboveground Biomass

[29] In the field, we observed mixed A soil horizons of fairly uniform depth [Yoo *et al.*, 2011] and no evidence of overland flow or ravelling processes, even during the 2009 field season when we visited the site after a fire. The entire area studied is forested, and we observed a number of uprooted trees and associated surface pits. These field observations suggest that slope-dependent sediment transport on hilltops is dominated by vegetation turnover in the Feather River region, although we cannot rule out rheologic creep as a contributing mechanism [e.g., McKean *et al.*, 1993].

[30] Vegetation properties were compared along two prominent ridges in the granodiorite and the metavolcanics to determine whether the differing distributions of hilltop curvature could be explained by vegetation controlling the sediment transport coefficient (Figure 11). These ridgelines were selected as the only hilltops bound on both sides by

the main tributary channels. On these ridges, hilltops are sharp (more negative C_{HT} values indicate sharper hilltops and imply more rapid erosion): mean C_{HT} for granodiorite is -0.067 m^{-1} and -0.12 m^{-1} for metavolcanics (Figure 12), indicating that these sites have likely responded to baselevel lowering (though they may still be adjusting). We find that vegetation on the two ridges has remarkably similar density ratios $V_{\text{dens}} \sim 0.8$ yet exhibit differences in canopy height (Figure 11). The mean height values from profiles along the length of each ridgeline are similar on both ridges ($V_{\text{mean}} = 7.9 \pm 4.9\text{ m}$ and $8.0 \pm 3.5\text{ m}$ for ridges in the granodiorite and metavolcanics, respectively).

6. Discussion

6.1. Calibrating the Sediment Transport Coefficient

[31] To compare estimates of the sediment transport coefficient D between lithologies, we sampled hilltop curvature on all ridges within 500 m of reaches of the Feather River, Cascade River, or Little North Fork River that are downstream of knickpoints (Figure 4) where the long-term erosion rate is estimated to be c. 250 mm ka^{-1} [Riebe *et al.*, 2000; Wakabayashi and Sawyer 2001; Hurst *et al.*, 2012]. The results were binned to produce histograms of hilltop

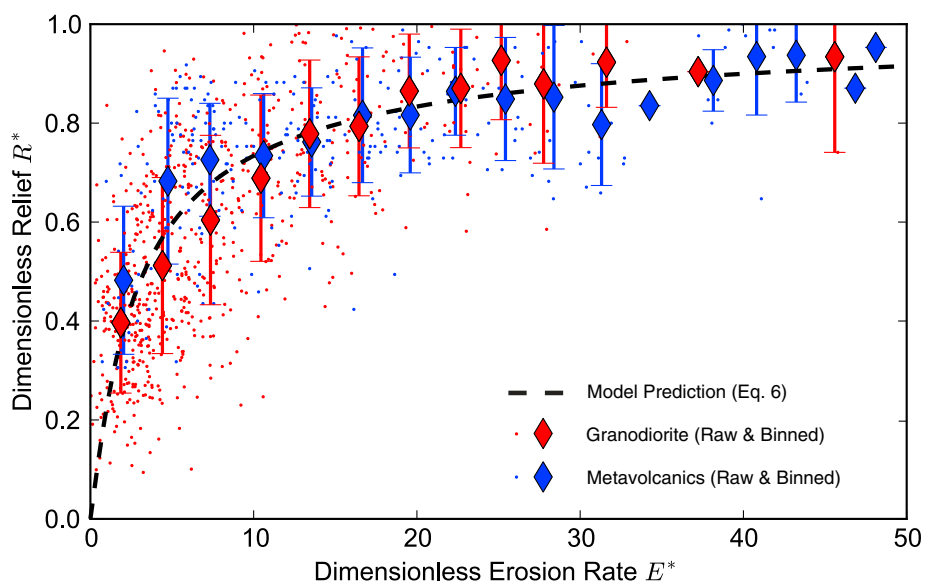


Figure 8. Non-dimensional erosion rate (E^*) and relief (R^*) calculated from topographic metrics following equations (5b) and (6b) for hilltops in the granodiorite (red) and metavolcanics (blue), using maximum likelihood estimated values for S_C of 0.79 and 0.85, respectively. Data are binned into regularly spaced bins in E^* . Black dashed line shows theoretical relationship predicted by equation (6a) for steadily eroding hillslopes. Non-dimensional analysis effectively normalizes the data from Figure 7 for variation in hillslope length. Hillslopes in the metavolcanics tend to be steeper for a given erosion rate despite correcting for hillslope length, suggesting a greater number of hillslopes undergoing transient adjustment were sampled in the metavolcanics (see text for further discussion).

curvature by lithology (Figure 12). Hilltops tend to be much sharper (curvature more negative) in the metavolcanics than in the granodiorite. Following equation (4), sharper hilltops can result from increased erosion rate E or reduced sediment transport efficiency D . We assume that proximal to the Feather, Cascade, and Little North Fork Rivers, downstream of knick zones (see Figure 4), the landscape has responded to accelerated incision such that erosion rates are equilibrated. We use median values and median absolute deviation to estimate D . Assuming $\rho_s / \rho_r = 0.5$ (a ratio that has been demonstrated for some other granitic field sites [e.g., Heimsath *et al.*, 2000; Riggins *et al.*, 2011]) and $E = 250 \text{ mm ka}^{-1}$, we solve equation (4) for D . In the granodiorite, $D = 8.8 \pm 3.3 \text{ m}^2 \text{ ka}^{-1}$. In the metavolcanics, hilltop curvature tends to be higher (more negative) (Figure 12), predicting a lower diffusivity of $D = 4.8 \pm 1.8 \text{ m}^2 \text{ ka}^{-1}$. The result from the granodiorite is similar to the value of $D = 8.0 \text{ m}^2 \text{ ka}^{-1}$ reported by Hurst *et al.* [2012] for granitoid lithologies in this field site based on data in Figure 2. The sediment transport rates reported here are dependent on the assumption that erosion rates are the same in parts of the landscape that are most likely to be adjusted to increased incision.

6.2. Applicability of Sediment Transport Models

[32] Much of the topographic analysis above has been carried out assuming that hillslope sediment transport is well approximated as a non-linear function of local slope (equation (3)). This model is assumed to be applicable to the Feather River since hilltop curvature varies linearly with erosion rate [Hurst *et al.*, 2012]. Models similar to equation (3) in which sediment flux is also a product of soil depth

(i.e., $D = D_d \times h$, where $D_d [\text{L T}^{-1}]$ is the transport coefficient for depth-dependent transport and $h [\text{L}]$ is soil depth) predict that hilltop curvature will vary non-linearly with erosion rate, becoming extremely sensitive to changes in E when E is high [Roering, 2008]. Field measurements of soil depth were invariant on hillslopes above, at, and just below a prominent break in slope that separates the relict landscape from the steep topography in an area of tonalite ~10 km to the south of the study area [Yoo *et al.*, 2011]. This implies that soil thickness is set primarily by the depth of root action in this forested landscape. However, there are local patches of bare bedrock on upland surfaces underlain by granitoids. These occur either (i) in broad patches on the gently eroding relict surface or (ii) immediately adjacent to the Feather River, in large single patches of exposure below the break in slope separating the steepened landscape from the relict topography. This may be attributed to particularly resistant patches of granitoid and/or a negative feedback whereby stripping of soil inhibits further soil production [e.g., Furbish and Fagherazzi, 2001]. There is also patchy bedrock outcrops below knickpoints in the channel system, even in the predominantly soil-mantled areas this study has focused on, and a recent study demonstrated that the amount of rock exposure on hillslopes increases with erosion rate across a wide range of erosion rates (10–1000 mm ka^{-1}) [DiBiase *et al.*, 2012]. The extent to which patchy bedrock emergence limits the application of non-linear (and/or depth-dependent) hillslope sediment transport models remains unclear. DiBiase *et al.* [2012] also demonstrated that mean hillslope gradient measured from high resolution topography may continue to increase with erosion rates beyond those at which studies using coarser DEMs have suggested that hillslope gradients become limited [e.g., Binnie *et al.*, 2007;

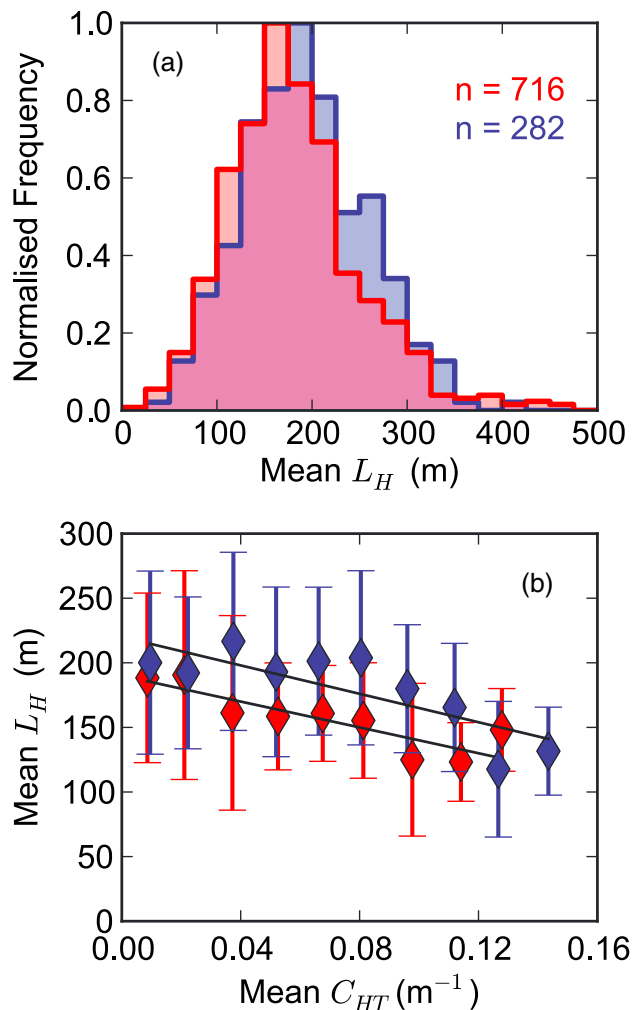


Figure 9. (a) Frequency of hillslope length L_H for the granodiorite (red) and metavolcanics (blue), normalized by the maximum frequency. Maximum frequency occurs at $L_H = 150\text{--}175\text{ m}$ in the granodiorite and $L_H = 175\text{--}200\text{ m}$ in the metavolcanics. Additionally, there are more short hillslopes in the granodiorite and more long hillslopes in the metavolcanics. A t -test reveals at 99% confidence that these two datasets are drawn from different populations. (b) Plot of C_{HT} (indicating relative erosion rate) versus L_H in granodiorite (red) and metavolcanics (blue). Black lines represent linear least-square fits to binned averages with $R^2 = 0.74$ and 0.66 , respectively. Hillslope lengths tend to shorten with increasing hilltop curvature (an indicator of erosion rates).

Ouimet et al., 2009; *DiBiase et al.*, 2010]. The relationship between C_{HT} and S presented in Figure 7 supports this, although we have limited data at high erosion rates (high C_{HT}). We do however stress that E^* vs. R^* curves in this landscape are similar to predictions based on the non-linear sediment transport model, suggesting this model provides a good description of hillslope morphology in the Feather River.

[33] Previously reported values for critical slope S_C in equation (3) vary between 0.8 and 1.25. *Roering et al.* [1999] performed forward modeling of a real landscape in the Oregon Coastal Range to calibrate a best fit value of 1.25. *DiBiase et al.* [2010] found that $S_C = 0.81$ provided a

better fit in the San Gabriel Mountains, California, by fitting hillslope morphology to the theoretical E^* vs. R^* curve. *Mattson and Bruhn* [2001] reported $S_C = 0.95$ in cohesionless sediment cut by fault scarps in the Wasatch Fault Zone, Utah, by comparing numerically modeled scarp profiles to modern scarp morphology. Through analyzing the non-dimensional form of hillslopes, best fit values for S_C in the Feather River region were 0.79 and 0.85 in granodiorite and metavolcanics, respectively, and similar to the median values of hillslope gradient in rapidly denuding regions of the landscape (Figure 10). In the context of equation (3), S_C represents a slope angle that cannot be attained since sediment flux becomes infinite at S_C . As such, there is discrepancy between our fitted S_C and the distribution of slope angles in the landscape shown in Figure 10. We hypothesize that our sampling approach may under-sample the steepest parts of the landscape, with hillslope traces terminating in debris flow channel heads, whilst the steepest hillslope gradients occur where there is patchy emergent bedrock on hillslopes proximal to the main stem channels. Equation (3) applies only to soil-covered hillslopes, whereas emergent bedrock will be capable of maintaining steeper slopes, limited by the mechanical strength of the rock face.

6.3. Transient Landscape Response

[34] In Figure 4, it can be observed that the transient erosion rate signal, represented in this case by a distinct convexity in the channel profile, has migrated further along the Little North Fork River than the Cascade River. All else being equal, we would expect knickpoints to propagate faster into weaker/less resistant lithologies [*Whipple and Tucker*, 1999], suggesting that the metavolcanics may be less resistant to fluvial erosion than the granodiorite. However, the Little North Fork is a slightly larger basin (120 km^2 compared to Cascade River 85 km^2). The tendency for hillslopes in the metavolcanics to have steep slopes at low hilltop curvature results in them plotting above the steady state line in Figure 8, and therefore, they may still be responding to accelerated incision [Hurst et al., 2012]. Hillslope morphology in the granodiorite conforms better to the steady state predictions (Figure 8). Hillslopes in the granodiorite may be able to keep pace with channel incision due to having a higher sediment transport coefficient [Roering et al., 2001b]. Additionally, since the knickpoint has not migrated as far into the granodiorite, it is likely propagating slower than in the metavolcanics. *Gallen et al.* [2011] demonstrated that the passing of a knickpoint results in hillslope steepening and an increase in hillslope relief immediately downstream; these results mirrored the theoretical predictions of *Mudd and Furbish* [2007]. However, with increasing distance downstream from the knickpoint, *Gallen et al.* [2011] found that these metrics begin to reduce again, suggesting that hillslopes are relaxing following the passing of a knickpoint and initial hillslope steepening. In the Feather River, we have been unable to observe such relaxation on hillslopes and are as yet unable to assert whether the increased erosion rates that have carved the Feather River canyon are a persistent response to a change in tectonic forcing or alternatively reflect a baselevel adjustment similar to that observed by *Gallen et al.*, [2011]. Such a problem has important bearing on the calibrated values of D , since we have assumed in section 6.1 that erosion rates are the same, and persistently

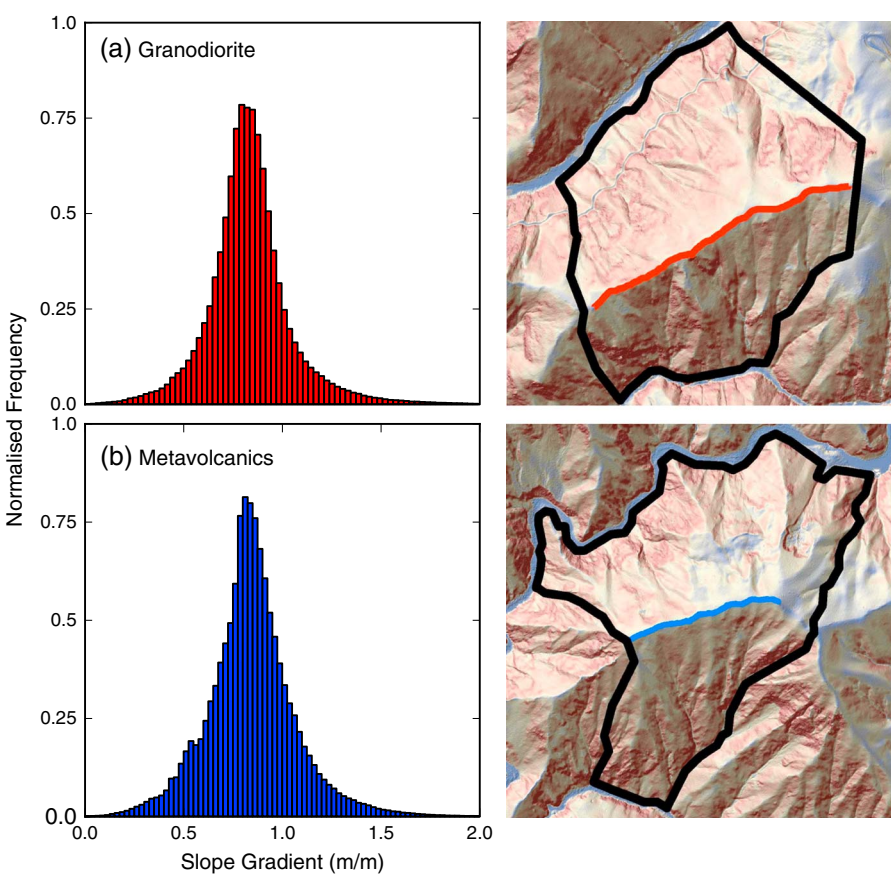


Figure 10. Distribution of hillslope gradients and area sampled for hillslopes in (a) Cascade Pluton and (b) Little North Fork metavolcanics. Slope calculated over 12 m window following Hurst *et al.* [2012]. For Cascade, mean slope is 0.84 and median slope is 0.83. For the Little North Fork, mean slope is 0.85 and median slope is 0.86.

high, in order to solve equation (4) to derive D . Analysis of cosmogenic radionuclides in cave sediments elsewhere in the Sierra Nevada suggests that the erosion history in the late Cenozoic is characterized by a pulse of incision moving through the landscape [Stock *et al.* 2004]. Incision is inferred to be a response to accelerated uplift in the late Cenozoic [Wakabayashi and Sawyer, 2001]. The likely mechanism of uplift is an isostatic response to delamination of an eclogite root beneath the mountain range [Saleeby and Foster, 2004; Jones *et al.*, 2004]. Therefore, it seems likely that uplift rates will decrease through time as new isostatic equilibrium is approached.

6.4. Hillslope Lengths and Drainage Density

[35] Hillslope lengths tend to be longer in the metavolcanics than in the granodiorite (Figure 9). A recent study by Perron *et al.* [2008] postulated that drainage density and its inverse, hillslope length, should be set by the relative efficiency of diffusive (hillslope) and advective (valley-forming) processes. Their analysis focused on low-relief settings, where hillslope processes could be assumed to be diffusive and sediment flux linearly related to slope, whilst valley-forming processes were dominated by channelization of overland flow. However, the present study was focused on a landscape responding to an order of magnitude increase in erosion rates, where zero-order basins may be

predominantly eroded by debris flows and hillslopes approach a threshold gradient as a process transition to landslide-dominated sediment transport occurs. Perron *et al.* [2009] demonstrated that such a relationship breaks down in rapidly denuding landscapes with steep planar hillslopes such as the Oregon Coastal Range.

[36] Hillslope length L_H in part controls slope steepness through setting the proportion of a hillslope that is planar and experiencing non-linearity in sediment transport [Roering *et al.*, 2001b] (i.e., the longer the hillslope, the longer the proportion of its length that will be steep and planar). In the Feather River region, hillslope length decreases with erosion rate (assuming C_{HT} is a surrogate) (Figure 9). Mudd and Furbish [2005] demonstrated that hilltops may migrate when subject to differential erosion rate on either flank such that when erosion rate is raised on one side, the hillslope on that side increases its length. However, in their model, the extent of the drainage network was fixed, and an increase in hillslope length by divide migration was accommodated by shortening of the adjacent, low erosion rate hillslope. Contrary to the results presented here, drainage density (inverse of L_H) has been demonstrated to vary negatively with relief in steep, mountainous landscapes [Montgomery and Dietrich, 1988; Oguchi, 1997]. Such a result has been supported by analytical and numerical modeling studies which predict that where hillslope sediment transport is

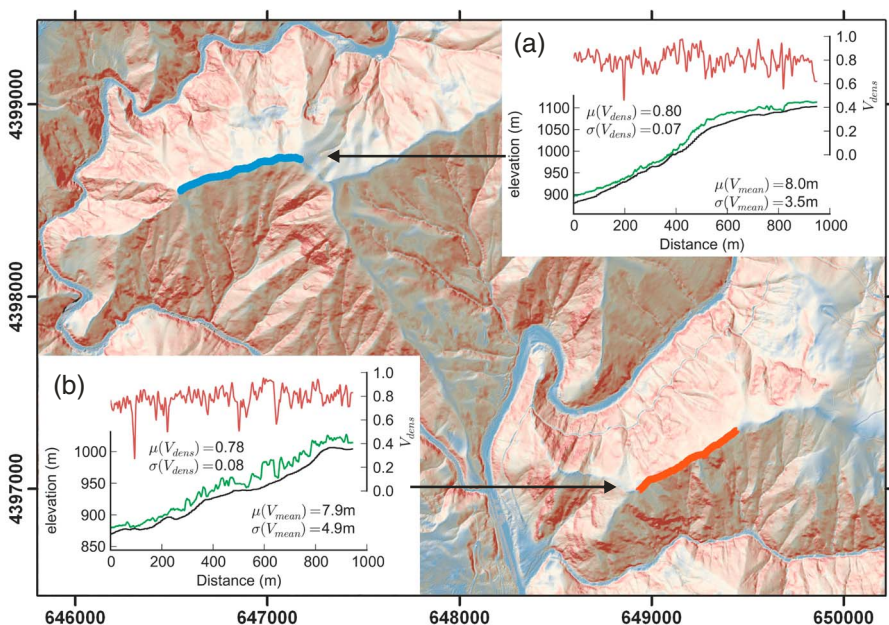


Figure 11. Comparison of vegetation properties for (a) Little North Fork ridge and (b) Cascade Ridge. Vegetation density (V_{dens}) is plotted in red, and mean canopy height (V_{mean}) is the difference in elevation between the ground surface (black) and mean vegetation elevation (green). Both vegetation parameters are similar between the two sites, but canopy height is more variable on cascade ridge due to the presence of several large trees. Background image is shaded slope map similar to Figure 2. The spatial reference system is UTM Zone 10N with spatial units in meters.

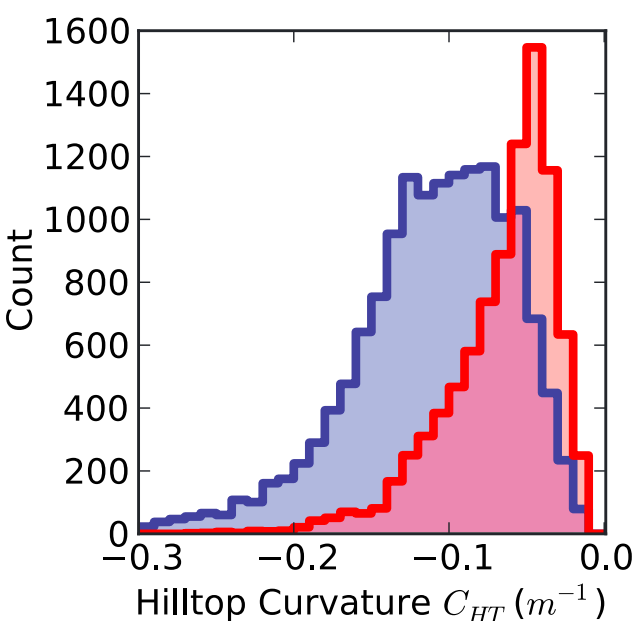


Figure 12. Histogram of hilltop curvatures extracted from hilltops adjacent to the Feather River, Cascade River, and Little North Fork River. Distributions are negatively skewed, and median values (median absolute deviation reported as error range) are $-0.105 \pm 0.034 \text{ m}^{-1}$ and $-0.057 \pm 0.019 \text{ m}^{-1}$ for hilltops in the metavolcanics (blue) and granodiorite (red), respectively.

dominated by landsliding, there should be an inverse relationship between drainage density and topographic relief [Howard, 1997; Tucker and Bras, 1998]. These studies have focused on landscapes (real or otherwise) that are assumed to be adjusted to their boundary conditions. The Feather River is still responding to a transient erosion signal, and as such, the patterns observed here may only be associated with processes of landscape response. In landscapes experiencing rapid erosion, where coupled landslide and debris-flow processes are likely to be the dominant erosion processes on hillslopes and in valleys respectively, drainage density is likely to be influenced by factors governing the frequency and magnitude of landslide events and the potential for these events to erode valleys as they translate into debris flows and scour the substrate [e.g., Stock and Dietrich, 2006]. In such settings, it may therefore be difficult to isolate the relative efficiencies of hillslope- and valley-forming processes. We find that hillslopes tend to get shorter with increased erosion rate in the Feather River and speculate that this may be due to an increase in debris flow frequency, allowing the valley-forming process to be more efficient at high erosion rates, so that valley heads migrate further into the landscape.

6.5. Mechanisms for Lithologic Control on Hillslope Sediment Transport

[37] Several workers have suggested that lithology may be important in setting D [e.g., McKean et al., 1993; Yoo et al., 2005], but as yet, we have limited quantitative understanding of such a relationship [c.f. Furbish et al., 2009]. This is in part due to an inability to isolate lithologic control from

that of climate, vegetation, and bioturbation. Here we have demonstrated that D varies by a factor of two between two landscapes underpinned by different lithologies, despite similarity in vegetation, and presumably climate, given their spatial proximity and similar range in altitude. The sediment transport coefficient is not directly controlled by lithology, rather by the characteristics of the soil produced and the processes that act to transport sediment, which are in turn influenced by lithology. We have demonstrated that LiDAR metrics for AGB are similar between the two lithologies on hilltops; therefore, energy expended in root growth/decay and tree throw should be similar, yet the amount of soil moved per transport event must differ. Future research should attempt to quantify mechanical properties of bedrock and chemical weathering in settings where D can be determined, and a number of possible mechanisms by which lithology may influence sediment transport can be anticipated.

[38] The chemical and physical properties of soils are set by lithology, which influence the efficacy of sediment transport. Disparity in the degree of chemical and physical weathering in soil and saprolite may result in different volumes of material mobilized by tree throw and root growth. *Furbish et al.* [2009] derived a diffusion-like equation through describing the disturbing and settling motions of individual particles within a soil. They parameterized D as controlled by active soil depth, characteristic particle size, porosity (partially set by particle size), and a rate of particle activation (frequency of disturbance per unit time). The grain size distribution in a soil may then exert control on sediment transport efficiency by adjusting the mean free path length a grain can travel when disturbed or settling. Coarser grain size distributions have larger pore spaces and therefore facilitate longer travel distances per disturbance event. Rapid erosion rates lead to shorter residence times of soil material, and therefore, less time is available for the production of fine-grained weathering products such as clays and pedogenic crystalline iron [Mudd and Yoo, 2010; Yoo et al., 2011], and accelerated erosion rates are expected to result in a greater proportion of rock fragments in soils [Marshall and Sklar, 2011]. Furthermore, variation in grain size distributions may influence the hydrology [e.g., Poesen and Lavee, 1994], potentially impacting upon cyclical wetting/drying expansion/contraction within the soil. Because grain size distributions in soils are likely to be positively correlated with erosion rates, we also expect that D may increase with erosion rates. Therefore, the common assumption that D is independent of E (which we apply in equation (4)) may not hold for disturbance-driven sediment transport; if true, this would introduce significant complexity to efforts to utilize hillslope topography to predict erosion rates.

7. Conclusions

[39] Despite similar vegetation, the hillslope morphology in two distinct lithologies in the Feather River region of California varies significantly, with hillslopes in metamorphosed volcanic rocks tending to be steeper and longer than those in a granodiorite pluton. Variation of the sediment transport coefficient is inferred from hilltop curvature in rapidly eroding portions of the landscape, with the sediment transport coefficient being lower in metavolcanics ($4.8 \pm 1.8 \text{ m}^2 \text{ ka}^{-1}$) than in the granodiorite ($8.8 \pm 3.3 \text{ m}^2 \text{ ka}^{-1}$). The study area

is undergoing a transient adjustment to accelerated baselevel fall and therefore exhibits a large range in hilltop curvature (considered an indicator of erosion rate at steady state). Hillslope gradient increases monotonically with hilltop curvature until approaching a critical hillslope gradient S_C . The range of erosion rates facilitates estimation of S_C at 0.79 and 0.85 in the granodiorite and metavolcanics, respectively. Hillslopes on metavolcanics tend to have a steeper mean gradient at low hilltop curvature, indicating that they are in a transient stage of adjustment to increased erosion rate. Hillslope lengths get shorter as hilltop curvature increases, suggesting that drainage density is coupled to the rate of erosion during adjustment. We conclude that lithologic variability in a landscape can influence rates of sediment transport, influencing the topographic form of hillslopes and that lithology influences the degree of landscape dissection.

[40] **Acknowledgments.** This work was supported by a National Environmental Research Council (NERC) Doctoral Training Grant NE/G524128/1 awarded to M. D. Hurst and NERC NE/H001174/1 to S. M. Mudd. Funding for this work was also provided by the National Science Foundation EAR0819064 (Empirical and Theoretical Integration of Geochemical and Morphologic Evolution of Soil-Covered Hillslopes: Responses to Channel Incision) to K. Yoo and S. M. Mudd for which LiDAR topographic data were acquired by the National Center for Airborne Laser Mapping. We are grateful to Edward Mitchard for guidance on estimating AGB from discrete return LiDAR data and Lyndsey Mackay for GIS guidance. We also thank the associate editor Simon Brocklehurst, Josh Roering, and two anonymous reviewers whose comments and insights helped refine and improve this contribution. We are particularly grateful to editor Alex Densmore for his insights and diligence.

References

- Ahnert, F. (1970), Functional relationships between denudation, relief, and uplift in large mid-latitude drainage basins, *Am. J. Sci.*, 268(3), 243–263, doi:10.2475/ajs.268.3.243.
- Almond, P. C., J. J. Roering, M. W. Hughes, F. S. Lutter, and C. Lebouteiller (2008), Climatic and anthropogenic effects on soil transport rates and hillslope evolution, *Sediment Dynamics in Changing Environments*, Christchurch, New Zealand: IAHS Publication, 325, 417–424.
- Anderson, R. S. (1994), Evolution of the Santa Cruz Mountains, California, through tectonic growth and geomorphic decay, *J. Geophys. Res.*, 99(B10), 20161–20179, doi:10.1029/94JB00713.
- Andrews, D. J., and R. C. Bucknam (1987), Fitting degradation of shoreline scarps by a nonlinear diffusion-model, *J. Geophys. Res.*, 92(B12), 12857–12867, doi:10.1029/JB092iB12p12857.
- Armitage J. J., R. A. Duller, A. C. Whittaker, and P. A. Allen (2011), Transformation of tectonic and climatic signals from source to sediment archive, *Nature Geosci.*, 4, 231–235.
- Arrowsmith, J. R., D. D. Rhodes, and D. D. Pollard (1998), Morphologic dating of scarps formed by repeated slip events along the San Andreas Fault, Carrizo Plain, California, *J. Geophys. Res.* 103(B5), 10131–10160, doi:10.1029/98JB00505.
- Avouac, J. P., and G. Peltzer (1993), Active tectonics in southern Xingjiang, China: Analysis of terrace rise and normal fault scarp degradation along the Hotan-Qira fault system, *J. Geophys. Res.*, 98, 21773–21807, doi:10.1029/93JB02172.
- Avouac, J. P., P. Tappognon, M. Bai, H. You, and G. Wang (1993), Active thrusting and folding along the northern Tien-Shan and late Cenozoic rotation of the Tarim relative to Dzungaria and Kazakhstan, *J. Geophys. Res.* 98(B4), 6755–6804, doi:10.1029/92JB01963.
- Begin, Z. B. (1992), Application of quantitative morphologic dating to paleoseismicity of the northwestern Negev, Israel, *Isr. J. Earth Sci.*, 41, 95–103.
- Binnie, S. A., W. M. Phillips, M. A. Summerfield, and L. K. Fifield (2007), Tectonic uplift, threshold hillslopes, and denudation rates in a developing mountain range, *Geology*, 35(8), 743–746, doi:10.1130/G23641A.1v.
- Bowman, D., and R. Gerson (1986), Morphology of the latest Quaternary surface-faulting in the Gulf of Elat region, eastern Sinai, *Tectonophysics*, 128, 97–119, doi:10.1016/0040-1951(86)90310-0.
- Bowman, D., and T. Gross (1989), Neotectonics in the northern Arava: Research report to the Israel Department of Energy (in Hebrew).
- Burbank, D. W., J. Leland, E. Fielding, R. S. Anderson, N. Brozovic, M. R. Reid, and C. Duncan (1996), Bedrock incision, rock uplift and threshold

- hillslopes in the northwestern Himalayas, *Nature*, 379(6565), 505–510, doi:10.1038/379505a0.
- Burke, B. C., A. M. Heimsath, and A. F. White (2007), Coupling chemical weathering with soil production across soil-mantled landscapes, *Earth Surf. Proc. Land.*, 32, 853–873.
- Carretier, S., J.-F. Ritz, J. Jackson, and A. Bayasgalan (2002), Morphological dating of cumulative reverse fault scarps: Examples from the Gurvan Bogd fault system, Mongolia, *Geophys. J. Int.*, 148, 256–277, doi:10.1046/j.1365-246X.2002.01599.X.
- Cecil, M. R., M. N. Ducea, P. W. Reiners, and C. G. Chase (2006), Cenozoic exhumation of the northern Sierra Nevada, California, from (U-Th)/He thermochronology, *Geol. Soc. Am. Bull.*, 118(11–12), 1481–1488, doi:10.1130/B25876.1.
- Clark, D. H. (1995), Extent, timing, and climatic significance of latest Pleistocene and Holocene glaciation in the Sierra Nevada, California, 193 pp, University of Washington, Seattle, WA.
- Clark, M. L., D. A. Roberts, J. J. Ewel, and D. B. Clark (2011), Estimation of tropical rain forest aboveground biomass with small-footprint lidar and hyperspectral sensors, *Remote Sens. Environ.*, 115, 2931–2942, doi:10.1016/j.rse.2010.08.029.
- Clarke, B. A., and D. W. Burbank (2010), Bedrock fracturing, threshold hillslopes, and limits to the magnitude of bedrock landslides, *Earth Planet. Sci. Lett.*, 297(3–4), 577–586.
- Clarke, B. A., and D. W. Burbank (2011), Quantifying bedrock fracture patterns within the shallow subsurface: Implications for rock mass strength, bedrock landslides, and erodibility, *J. Geophys. Res.*, 116, F04009, doi:10.1029/2011JF001987.
- Colman, S. M., and K. Watson (1983), Ages estimated from a diffusion equation model for scarp degradation, *Science*, 221, 263–265, 10.1126/science.221.4607.263.
- Constantine, J. A., M. J. Schelhaas, E. Gabet, and S. M. Mudd (2012), Limits of windthrow-driven hillslope sediment flux due to varying storm frequency and intensity, *Geomorph.*, 175–176, 66–73, doi:10.1016/j.geomorph.2012.06.022.
- Culling, W. E. H. (1960), Analytical theory of erosion, *J. Geol.*, 68(3), 336–344.
- Daly, C., G. Taylor, and W. Gibson, (1997), The PRISM approach to mapping precipitation and temperature, 10th Conf. on Applied Climatology, Reno, NV, Amer. Meteor. Soc., 10–12.
- Davis, W. M. (1892), The convex profile of badland divides, *Science*, 20, 245.
- Day, H. W., and M. E. Bickford (2004), Tectonic setting of the Jurassic Smartville and Slate Creek complexes, northern Sierra Nevada, California, *Geol. Soc. Am. Bull.*, 116(11/12), 1515–1528, doi:10.1130/B25416.1.
- DiBiase, R. A., K. X. Whipple, A. M. Heimsath, and W. B. Quimet (2010), Landscape form and millennial erosion rates in the San Gabriel Mountains, CA, *Earth Planet. Sci. Lett.*, 289(1–2), 134–144, doi:10.1016/j.epsl.2009.10.036.
- DiBiase, R. A., A. M. Heimsath, and K. X. Whipple (2012), Hillslope response to tectonic forcing in threshold landscapes, *Earth Surf. Proc. Land.*, 37(8), 855–865, doi:10.1002/esp.3205.
- Dietrich, W. E., D. G. Bellugi, L. S. Sklar, and J. D. Stock (2003), Geomorphic transport laws for predicting landscape form and dynamics, in Prediction in Geomorphology, *Geophys. Monogr. Ser.*, vol. 135, edited by P. R. Wilcock, and R. M. Iverson, pp. 103–132, AGU, Washington, D.C.
- Dixon, J. L., A. M. Heimsath, and R. Amundson (2009), The critical role of climate and saprolite weathering in landscape evolution, *Earth Surf. Proc. Land.*, 34, 1507–1521, doi:10.1002/esp.1836.
- Donoghue D. N. M., and P. J. Watt (2006), Using LiDAR to compare forest height estimates from IKONOS and Landsat ETM+ data in Sitka spruce plantation forests, *Int. J. Remote Sens.*, 27(11), 2161–2175, doi:10.1080/01431160500396493.
- Duller, R. A., A. C. Whittaker, J. J. Fedele, A. L. Whitchurch, J. Springett, R. Smithells, S. Fordyce, and P. A. Allen (2010), From grain size to tectonics, *J. Geophys. Res.*, 115, F03022, doi:10.1029/2009JF001495.
- Dunne, T., D. V. Malmon, and S. M. Mudd (2010), A rain splash transport equation assimilating field and laboratory measurements, *J. Geophys. Res.*, 115, F01001, doi:10.1029/2009JF001302.
- Enzel, Y., R. Amit, N. Porat, E. Zilberman, and B. J. Harrison (1996), Estimating the ages of fault scarps in the Arava, Israel, *Tectonophysics*, 253, 305–317, doi:10.1016/0040-1951(95)00072-0.
- Foufoula-Georgiou, E., V. Ganti, and W. E. Dietrich (2010), A nonlocal theory of sediment transport on hillslopes, *J. Geophys. Res.*, 115, F00A16, doi:10.1029/2009JF001280.
- Furbish, D. J. and S. Fagherazzi (2001), Stability of creeping soil and implications for hillslope evolution, *Water Resour. Res.*, 37(10), 2607–2618, doi:10.1029/2001WR000239.
- Furbish, D. J., P. K. Haff, W. E. Dietrich, and A. M. Heimsath (2009), Statistical description of slope-dependent soil transport and the diffusion-like coefficient, *J. Geophys. Res.*, 114, F00A05, doi:10.1029/2009JF001267.
- Gabet, E. J. (2000), Gopher bioturbation: Field evidence for non-linear hillslope diffusion, *Earth Surf. Proc. Land.*, 25, 1419–1428, doi:10.1002/1096-9837(200012)25:13<1419::AID-ESP148>3.0.CO;2-1.
- Gabet, E. J. (2003), Sediment transport by dry ravel, *J. Geophys. Res.*, 108(B1), 2049, doi:10.1029/2001JB001686.
- Gabet, E. J., O. J. Reichman, and E. W. Seabloom (2003), The effects of bioturbation on soil processes and sediment transport, *Annu. Rev. Earth Planet. Sci.*, 31, 249–273, doi:10.1146/annurev.earth.31.100901.141314.
- Gabet, E. J., and S. M. Mudd (2010), Bedrock erosion by root fracture and tree throw: A coupled biogeomorphic model to explore the humped soil production function and the persistence of hillslope soils, *J. Geophys. Res.*, 115, F04005, doi:10.1029/2009JF001526.
- Gallen, S. F., K. W. Wegmann, K. L. Frankel, S. Hughes, R. Q. Lewis, N. Lyons, P. Paris, K. Ross, J. B. Bauer, and A. C. Witt (2011), Hillslope response to knickpoint migration in the Southern Appalachians: Implications for the evolution of post-orogenic landscapes, *Earth Surf. Proc. Land.*, 36, 1254–1267, doi:10.1002/esp.2150.
- Gilbert, G. K. (1909), The convexity of hilltops, *J. Geol.*, 17(4), 344–350.
- Granger, D. E., C. S. Riebe, J. W. Kirchner, and R. C. Finkel (2001), Modulation of erosion on steep granitic slopes by boulder armoring, as revealed by cosmogenic ^{26}Al and ^{10}Be , *Earth Planet. Sci. Lett.*, 186, 269–281, doi:10.1016/S0012-821X(01)00236-9.
- Hall, S. A., I. C. Burke, D. O. Box, M. R. Kaufmann, and J. M. Stoker (2005), Estimating stand structure using discrete-return lidar: An example from low density, fire-prone ponderosa pine forests, *Forest Ecol. Manag.*, 208, 189–209, doi:10.1016/j.foreco.2004.12.001.
- Hanks, T. C., R. C. Bucknam, K. R. Lajoie, and R. E. Wallace (1984), Modification of wave-cut and faulting-controlled landforms, *J. Geophys. Res.*, 89(NB7), 5771–5790, doi:10.1029/JB089iB07p05771.
- Hanks, T. C., and R. E. Wallace (1985), Morphological analysis of the Lake Lahontan and beachfront fault scarps, Pershing County, Nevada, *Bull. Seismol. Soc. Am.*, 75, 835–846.
- Hanks, T. C., and D. J. Andrews (1989), Effect of far-field slope on morphologic dating of scarp-like landforms, *J. Geophys. Res.*, 94, 565–573, doi:10.1029/JB094iB01p00565.
- Hanks, T. C. (2000), The age of scarp-like landforms from diffusion-equation analysis, in Quaternary Geochronology: Methods and Applications, edited by J. Stratton Noller, J. M. Sowers, and W. R. Letts, pp. 313–338, AGU, Washington, D.C.
- Heimsath, A. M., J. Chappell, W. E. Dietrich, K. Nishiizumi, and R. Finkel (2000), Soil production on a retreating escarpment in southeastern Australia, *Geology*, 28 (9), 787–790, doi:10.1130/0091-7613(2000)28<787:SPOARE>2.0.CO;2.
- Heimsath, A. M., D. J. Furbish, W. E. Dietrich (2005), The illusion of diffusion: Field evidence for depth-dependent sediment transport, *Geology*, 33(12), 949–952, doi:10.1130/G21868.1.
- Hijmans, R. J., S. E. Cameron, J. L. Parra, P. G. Jones, and A. Jarvis (2005), Very high resolution interpolated climate surfaces for global land areas, *Int. J. Climatol.*, 25, 1965–1978, doi:10.1002/joc.1276.
- Holmgren, J., M. Nilsson, and H. Olsson (2003), Estimation of tree height and stem volume on plots using airborne laser scanning, *Forest Sci.*, 49(3), 419–428.
- Howard, A. D. (1994), A detachment-limited model of drainage-basin evolution, *Water Resour. Res.*, 30(7), 2261–2285, doi:10.1029/94WR00757.
- Howard, A. D. (1997), Badland morphology and evolution: Interpretation using a simulation model, *Earth. Surf. Proc. Land.*, 22, 211–227, doi:10.1002/(SICI)1096-9837(199703)22:3<211::AID-ESP749>3.0.CO;2-E.
- Hughes, M. W., P. C. Almond, and J. J. Roering (2009), Increased sediment transport via bioturbation at the last glacial-interglacial transition, *Geology*, 37(10), 919–922, doi:10.1130/G30159A.1
- Hurst, M. D., S. M. Mudd, R. Walcott, M. Attal, and K. Yoo (2012), Using hilltop curvature to derive the spatial distribution of erosion rates, *J. Geophys. Res.*, 117, F02017, doi:10.1029/2011JF002057.
- Jones, C. H., G. L. Farmer, and J. Unruh (2004), Tectonics of Pliocene removal of lithosphere of the Sierra Nevada, California, *Geol. Soc. Am. Bull.*, 116(11/12), 1408–1422, doi:10.1130/B25397.1.
- Joetsna, R., and P. K. Haff (1997), Microtopography as an indicator of modern hillslope diffusivity in arid terrain, *Geology*, 25, 695–698, doi:10.1130/0091-7613(1997)025<0695:MDIOTH>2.0.CO;2.
- Jungers, M. C., P. R. Bierman, A. Matmon, K. Nichols, J. Larsen, and R. Finkel (2009), Tracing hillslope sediment production and transport with in situ and meteoric ^{10}Be , *J. Geophys. Res.*, 114, F04020, doi:10.1029/2008JF001086.
- Korup, O. (2008), Rock type leaves topographic signature in landslide-dominated mountain ranges, *Geophys. Res. Lett.*, 35, L11402, doi:10.1029/2008GL034157.
- Korup, O., and F. Schlunegger (2009), Rock-type control on erosion-induced uplift, eastern Swiss Alps, *Earth Planet. Sci. Lett.*, 278, 278–285, doi:10.1016/j.epsl.2008.12.012.
- Larsen, I. J., and D. R. Montgomery (2012), Landslide erosion coupled to tectonics and river incision, *Nat. Geosci.*, doi:10.1038/ngeo1479.
- Lashermes, B., E. Foufoula-Georgiou, and W. E. Dietrich (2007), Channel network extraction from high resolution topography using wavelets, *Geophys. Res. Lett.*, 34, L23S04, doi:10.1029/2007GL031140.

HURST ET AL.: LITHOLOGIC CONTROL ON HILLSLOPE RESPONSE

- Lea, N. J. (1992), An aspect-driven kinematic routing algorithm, in Overland Flow: Hydraulics and Erosion Mechanics, edited by A. J. Parsons and A. D. Abrahams, pp. 393–407, UCL Press, London.
- Lefsky, U.K., M. A., W. B. Cohen, D. J. Harding, G. G. Parker, S. A. Acker, and S. T. Gower (2002), Lidar remote sensing of above-ground biomass in three biomes, *Glob. Ecol. Biogeogr.*, *11*, 393–399, doi: 10.1046/j.1466-822x.2002.00303.X.
- Marshall, J. A., and L. S. Sklar (2011), Mining soil databases for landscape-scale patterns in the abundance and size distribution of hillslope rock fragments, *Earth Surf. Proc. Land.*, doi:10.1002/esp.2241.
- Martin, Y., and M. Church (1997), Diffusion in landscape development models: On the nature of basic transport relations, *Earth. Surf. Proc. Land.*, *22*, 273–279, doi: 10.1002/(SICI)1096-9837(199703)22:3<273::AID-ESP755>3.0.CO;2-D.
- Mattson, A., and R. L. Bruhn (2001), Fault slip rates and initiation age based on diffusion equation modelling: Wasatch Fault Zone and eastern Great Basin, *J. Geophys. Res.*, *106*(B7), 13739–13750, doi:10.1029/2001JB900003.
- McKean, J. A., W. E. Dietrich, R. C. Finkel, J. R. Southon, and M. W. Caffee (1993), Quantification of soil production and downslope creep rates from cosmogenic ^{10}Be accumulations on a hillslope profile, *Geology*, *21*(4), 343–346.
- Molnar, P., R. S. Anderson, and S. P. Anderson (2007), Tectonics, fracturing of rock, and erosion, *J. Geophys. Res.*, *112*, F03014, doi:10.1029/2005JF000433.
- Montgomery, D. R., and W. E. Dietrich (1988), Where do channels begin?, *Nature*, *336*(6196), 232–234, doi:10.1038/336232a0.
- Moosdorf, N., J. Hartmann, and H. H. Dürr (2010), Lithological composition of the North American continent and implications of lithological map resolution for dissolved silica flux modelling, *Geochem. Geophys. Geosyst.*, *11*, Q11003, doi:10.1029/2010GC003259.
- Mudd, S.M., and Furbish, D.J., (2004), Influence of chemical denudation on hillslope morphology, *J. Geophys. Res.: Earth Surf.*, *109*, F02001, doi: 10.1029/2003JF000087.
- Mudd, S. M., and D. J. Furbish (2005), Lateral migration of hillcrests in response to channel incision in soil-mantled landscapes, *J. Geophys. Res.*, *110*, F04026, doi:10.1029/2005JF000313.
- Mudd, S. M., and D. J. Furbish (2007), Responses of soil-mantled hillslopes to transient channel incision rates, *J. Geophys. Res.* *112*, F03S18, doi: 10.1029/2006JF000516.
- Mudd, S. M., and K. Yoo (2010), Reservoir theory for studying the geochemical evolution of soils, *J. Geophys. Res.*, *115*, F03030, doi: 10.1029/2009JF001591.
- Naesset, E. (1997), Determination of mean tree height of forest stands using airborne laser scanner data, *ISPRS J. Photogramm.*, *52*, 49–56.
- Nash, D. (1980a), Forms of bluffs degraded for different lengths of time in Emmet County, Michigan, U.S.A., *Earth Surf. Proc.*, *5*, 331–345, doi: 10.1002/esp.3760050405.
- Nash, D. B. (1980b), Morphologic dating of degraded normal-fault scarps, *J. Geol.*, *88*(3), 353–360.
- Nash, D. B. (1984), Morphologic dating of fluvial terrace scarps and fault scarps near West Yellowstone, Montana, *Geol. Soc. Am. Bull.*, *95*, 1413–1424, doi:10.1130/0016-7606(1984)95<1413:MDOFTS>2.0.CO;2.
- Nilsson, M. (1996), Estimation of tree heights and stand volume using an airborne lidar system, *Remote Sens. Environ.*, *56*, 1–7.
- Niviere, B. and G. Marquis (2000), Evolution of terrace risers along the upper Rhine graben inferred from morphologic dating methods: Evidence of climatic and tectonic forcing, *Geophys. J. Int.*, *141*, 577–594, doi: 10.1046/j.1365-246x.2000.00123.X.
- Oguchi, T. (1997), Drainage density and relative relief in humid steep mountains with frequent slope failure, *Earth Surf. Process. Land.*, *22*, 107–120, doi: 10.1002/(SICI)1096-9837(199702)22:2<107::AID-ESP680>3.0.CO;2-U.
- Ouimet, W. B., K. X. Whipple, and D. E. Granger (2009), Beyond threshold hillslopes: Channel adjustment to base-level fall in tectonically active mountain ranges, *Geology*, *37*(7), 579–582, doi:10.1130/G30013A.1.
- Owen, J. J., R. Amundson, W. E. Dietrich, K. Nishizumi, B. Sutter, and G. Chong (2010), The sensitivity of hillslope bedrock erosion to precipitation, *Earth Surf. Proc. Land.*, *36*(1), 117–135, doi:10.1002/esp.2083.
- Passalacqua, P., T. Do Trung, E. Foufoula-Georgiou, G. Sapiro, and W. E. Dietrich (2010), A geometric framework for channel network extraction from lidar: Nonlinear diffusion and geodesic paths, *J. Geophys. Res.*, *115*, F01002, doi:10.1029/2009JF001254.
- Pelletier, J. D., S. B. DeLong, A. H. Al-Suwaidi, M. Cline, Y. Lewis, J. L. Psillas, B. Yanites (2006), Evolution of the Bonneville shoreline scarp in west-central Utah: Comparison of scarp-analysis methods and implications for the diffusion model of hillslope evolution, *Geomorphology*, *74*, 257–270, doi:10.1016/j.geomorph.2005.08.008.
- Pelletier, J. D., and M. L. Cline (2007), Nonlinear slope-dependent sediment transport in cinder cone evolution, *Geology*, *35*(12), 1067–1070, doi: 10.1130/G23992A.1.
- Pelletier, J. D., et al. (2011) Calibration and testing of upland hillslope evolution models in a dated landscape: Banco Bonito, New Mexico, *J. Geophys. Res.*, *116*, F04004, doi:10.1029/2011JF001976.
- Perron, J. T., W. E. Dietrich, and J. W. Kirchner (2008), Controls on the spacing of first-order valleys, *J. Geophys. Res.* *113*, F04016, doi: 10.1029/2007JF000977.
- Perron, J. T., J. W. Kirchner, and W. E. Dietrich (2009), Formation of evenly spaced ridges and valleys, *Nature*, *460*, 502–505, doi:10.1038/nature08174.
- Petit, C., Y. Gunnell, N. Gonga-Saholiariliva, B. Meyer, and J. Se'guinot (2009), Faceted spurs at normal fault scarps: Insights from numerical modeling, *J. Geophys. Res.*, *114*, B05403, doi:10.1029/2008JB005955.
- Pierce, K. L., and S. M. Colman (1986), Effect of height and orientation (microclimate) on geomorphic degradation rates and processes, late-glacial terrace scarps in central Idaho, *Geol. Soc. Am. Bull.*, *97*, 869–885.
- Poesen, J., and H. Lavee (1994), Rock fragments in top soils: Significance and processes, *Catena*, *23*, 1–28, doi:10.1016/0341-8162(94)90050-7.
- Reneau, S. L. (1988), Depositional and erosional history of hollows: Application to landslide location and frequency, long-term erosion rates, and the effects of climatic change [Ph.D. thesis]: Berkeley, University of California, 328 p.
- Reneau, S. L., W. E. Dietrich, M. Rubin, D. J. Donahue, and A. J. T. Jull (1989), Analysis of hillslope erosion rates using dated colluvial deposits, *J. Geol.*, *97*, 45–63.
- Riebe, C. S., J. W. Kirchner, D. E. Granger, and R. C. Finkel (2000), Erosional equilibrium and disequilibrium in the Sierra Nevada, inferred from cosmogenic Al-26 and Be-10 in alluvial sediment, *Geology*, *28*(9), 803–806, doi:10.1130/0091-7613(2000)28<803:EEADIT>2.0.CO;2.
- Riebe, C. S., J. W. Kirchner, D. E. Granger, and R. C. Finkel (2001), Strong tectonic and weak climatic control of long-term chemical weathering rates, *Geology*, *29*(6), 511–514, doi:10.1130/0091-7613(2001)029<0511:STAWCC>2.0.CO;2.
- Riggins, S. G., R. S. Anderson, S. P. Anderson, and A. M. Tye (2011), Solving a conundrum of a steady-state hilltop with variable soil depths and production rates, Bodmin Moor, UK, *Geomorphology*, doi: 10.1016/j.geomorph.2010.12.023.
- Roering, J. J., J. W. Kirchner, and W. E. Dietrich (1999), Evidence for nonlinear, diffusive sediment transport on hillslopes and implications for landscape morphology, *Water Resour. Res.*, *35*(3), 853–870, doi: 10.1029/1998WR900090.
- Roering, J. J., J. W. Kirchner, L. S. Sklar, W. E. Dietrich (2001a), Hillslope evolution by nonlinear creep and landsliding: An experimental study, *Geology*, *29*(2), 143–146, doi:10.1130/0091-7613(2001)029<0143:HEBNCA>2.0.CO;2.
- Roering, J. J., J. W. Kirchner, and W. E. Dietrich (2001b), Hillslope evolution by nonlinear, slope-dependent transport: Steady state morphology and equilibrium adjustment timescales, *J. Geophys. Res.*, *106*(B8), 16499–16513, doi:10.1029/2001JB000323.
- Roering, J. J., P. Almond, P. Tonkin, and J. McKean (2002) Soil transport driven by biological processes over millennial time scales, *Geology*, *30*(12), 1115–1118. doi:10.1130/0091-7613(2002)030<1115:STDBBP>2.0.CO;2.
- Roering, J. J., P. Almond, P. Tonkin, and J. McKean (2004), Constraining climatic controls on hillslope dynamics using a coupled model for the transport of soil and tracers: Application to loess-mantled hillslopes, South Island, New Zealand, *J. Geophys. Res.*, *109*, F01010, doi: 10.1029/2003JF000034.
- Roering, J. J., and M. Gerber (2005), Fire and the evolution of steep, soil-mantled landscapes, *Geology*, *33*(5), 349–352.
- Roering, J. J., J. T. Perron, and J. W. Kirchner (2007), Functional relationships between denudation and hillslope form and relief, *Earth Planet. Sci. Lett.*, *264*(1–2), 245–258. doi:10.1016/j.epsl.2011.03.031.
- Roering, J. J. (2008) How well can hillslope evolution models “explain” topography? Simulating soil transport and production with high-resolution topographic data, *Geol. Soc. Am. Bull.*, *120*(9/10), 1248–1262. doi:10.1130/B26283.1
- Roering, J. J., J. Marshall, A. M. Booth, M. Mort, and Q. S. Jin (2010), Evidence for biotic controls on topography and soil production, *Earth Planet. Sci. Lett.*, *298*(1–2), 183–190.
- Rosenbloom, N. A., and R. S. Anderson (1994), Hillslope and channel evolution in a marine terraced landscape, Santa Cruz, California, *J. Geophys. Res.*, *99*(B7), 14013–14029, doi:10.1029/94JB00048.
- Saatchi, S. S., et al. (2011), Benchmark map of forest carbon stocks in tropical regions across three continents, *PNAS*, *108*(24), 9899–9904, doi:10.1073/pnas.1019576108.
- Saleeby, J., and Z. Foster (2004), Topographic response to mantle lithosphere removal in the southern Sierra Nevada region, California, *Geology*, *32*(3), 245–248, doi: 10.1130/G19958.1.
- Schaetzl, R. J., and L. R. Follmer (1990), Longevity of treethrow microtopography: Implications for mass wasting, *Geomorph.*, *3*(2), 113–123, doi:10.1016/0169-555X(90)90040-W.

- Schmidt, K. M., and D. R. Montgomery (1995), Limits to relief, *Science*, 270(5236), 617–620.
- Sklar, L. S., and W. E. Dietrich (2004), A mechanistic model for river incision into bedrock by saltating bed load, *Water Resour. Res.*, 40, W06301, doi:10.1029/2003WR002496.
- Small, E. E., R. S. Anderson, and G. S. Hancock (1999) Estimates of the rate of regolith production using ^{10}Be and ^{26}Al from an alpine hillslope, *Geomorph.*, 27, 131–150.
- Spelz, R. M., J. M. Fletcher, L. A. Owen, and M. W. Caffee (2008), Quaternary alluvial-fan development, climate and morphological dating of fault scarps in Laguna Salada, Baja California, Mexico, *Geomorphology*, 102, 578–594, doi:10.1016/j.geomorph.2008.06.001.
- Stock, J. D., and W. E. Dietrich (2006), Erosion of steepland valleys by debris flows, *Geol. Soc. Am. Bull.*, 118(9–10), 1125–1148, doi:10.1130/B25902.1.
- Stock, G. M., R. S. Anderson, and R. C. Finkel (2004), Pace of landscape evolution in the Sierra Nevada, California, revealed by cosmogenic dating of cave sediments, *Geology*, 32(3), 193–196, doi:10.1130/G20197.1.
- Tapponnier, P., et al. (1990), Active thrusting and folding in the Qilian-Shan, and decoupling between upper crust and mantle in northeastern Tibet, *Earth Planet. Sci. Lett.*, 97(3–4), 382–403, doi:10.1016/0012-821X(90)90053-Z.
- Tucker, G. E., and R. L. Bras (1998), Hillslope processes, drainage density and landscape morphology, *Water Resour. Res.*, 34(10), 2751–2764, doi:10.1029/98WR01474.
- Tucker, G. E., and D. N. Bradley (2010) Trouble with diffusion: Reassessing hillslope erosion laws with a particle-based model, *J. Geophys. Res.*, 115, F00A10, doi:10.1029/2009JF001264.
- Tucker, G. E., and G. R. Hancock (2010), Modelling landscape evolution, *Earth Surf. Proc. Land.*, 35, 28–50.
- Wahrhaftig, C., and J. H. Birman (1965), The Quaternary of the Pacific mountain system, in *The Quaternary of the United States*, edited by H. E. J. Wright, and D. G. Frey, pp. 299–340, Princeton University Press, New Jersey.
- Wakabayashi, J., and T. L. Sawyer (2001), Stream incision, tectonics, uplift, and evolution of topography of the Sierra Nevada, California, *J. Geol.*, 109(5), 539–562.
- Walther, S. C., J. J. Roering, P. C. Almond, M. W. Hughes (2009), Long-term biogenic soil mixing and transport in a hilly, loess-mantled landscape: Blue Mountains of southeastern Washington, *Catena*, 79, 170–178, doi:10.1016/j.catena.2009.08.003.
- Warbington, R. and D. Beardsley (2002), Estimates of old growth forests on the 18 National Forests of the Pacific Southwest Region, *USDA Forest Service*.
- Whipple, K. X., and G. E. Tucker (1999), Dynamics of the stream-power river incision model: Implications for height limits of mountain ranges, landscape response timescales, and research needs, *J. Geophys. Res.*, 104(B8), 17661–17674, doi:10.1029/1999JB900120.
- Whittaker, A. C., M. Attal, P. A. Allen (2010), Characterising the origin, nature and fate of sediment exported from catchments perturbed by active tectonics, *Basin Res.*, 22, 809–828.
- Yoo, K., R. Amundson, A. M. Heimsath, and W. E. Dietrich (2005), Process based model linking pocket gopher (*Thomomys bottae*) activity to sediment transport and soil thickness, *Geology*, 33(11), 917–920.
- Yoo, K., and S. M. Mudd (2008), Toward process-based modeling of geochemical soil formation across diverse landforms: A new mathematical framework, *Geoderma*, 146(1–2), 248–260.
- Yoo, K., B. Weinman, S. M. Mudd, M. Hurst, M. Attal, and K. Maher (2011), Evolution of hillslope soils: The geomorphic theater and the geochemical play, *Appl. Geochem.*, 26, S149–S153, doi:10.1016/j.apgeochem.2011.03.054.